Lawrence Berkeley National Laboratory

Title

Aerosol Fragmentation Driven by Coupling of Acid—Base and Free-Radical Chemistry in the Heterogeneous Oxidation of Aqueous Citric Acid by OH Radicals

Permalink

https://escholarship.org/uc/item/2hx5q6wq

Authors

Liu, Matthew J
Wiegel, Aaron A
Wilson, Kevin R
et al.

1 Aerosol Fragmentation Driven by Coupling of Acid-Base and Free Radical

2 Chemistry in the Heterogeneous Oxidation of Aqueous Citric Acid by OH

3 Radicals

4   Matthew J. Liu,[a,b] Aaron A. Wiegel,[a] Kevin R. Wilson,[†a] and Frances A. Houle[†a]

5   [a]Lawrence Berkeley National Laboratory, Chemical Sciences Division, Berkeley, CA, USA
6   94702
7   [b]University of California, Berkeley, Department of Chemical and Biomolecular Engineering,
8   Berkeley, CA, USA 94720

9[†] Authors to whom correspondence should be addressed:
10Frances A. Houle (fahoule@lbl.gov) and Kevin R. Wilson (krwilson@lbl.gov)
11

12**Abstract**

13A key uncertainty in the heterogeneous oxidation of carboxylic acids by hydroxyl radicals (OH)
14in aqueous phase aerosol is how the free radical reaction pathways might be altered by acid-base
15chemistry. In particular, if acid-base reactions occur concurrently with acyloxy radical formation
16and unimolecular decomposition of alkoxy radicals, there is a possibility that differences in
17reaction pathways impact the partitioning of organic carbon between the gas and aqueous phases.
18To examine these questions, a kinetic model is developed for the OH initiated oxidation of citric
19acid aerosol at high relative humidity. The reaction scheme, containing both free radical and
20acid-base elementary reaction steps with physically validated rate coefficients, accurately
21predicts the experimentally observed molecular composition, particle size, and average elemental
22composition of the aerosol upon oxidation. The difference between the two reaction channels
23centers on the reactivity of carboxylic acid groups. Free radical reactions mainly add functional
24groups to the carbon skeleton of neutral citric acid, because carboxylic acid moieties deactivate
25the unimolecular fragmentation of alkoxy radicals. In contrast, the conjugate carboxylate groups
26originating from acid-base equilibria activate both acyloxy radical formation and carbon-carbon
27bond scission of alkoxy radicals, leading to the formation of low molecular weight, highly
28oxidized products such as oxalic and mesoxalic acid. Subsequent hydration of carbonyl groups in
29the oxidized products increases the aerosol hygroscopicity and accelerates the substantial water
30uptake and volume growth that accompany oxidation. These results frame the oxidative lifecycle
31of atmospheric aerosol: it is governed by feedbacks between reactions that first increase the
32particle oxidation state, then eventually promote water uptake and acid-base chemistry. When
33coupled to free radical reactions, acid-base channels lead to formation of low molecular weight
34gas phase reaction products and decreasing particle size.
35
36
37
38

39

40**I.   Introduction**

41Sub-micron-sized atmospheric organic aerosols profoundly influence Earth's climate by 42interacting with incoming solar radiation and serving as cloud condensation nuclei, altering 43cloud formation and albedo.[1] The extent to which these processes occur is determined by the 44size, chemical composition, shape, and lifetime of the aerosol, making their characterization 45crucial for the predictive accuracy of air quality and climate models. However, describing the 46oxidative evolution (aging) of organic aerosol is difficult due to the extensive and complex 47chemical reactions that occur. The oxidation of organic aerosol is thought to have a major 48influence on particle composition and size, leading to numerous studies of the heterogeneous 49oxidation of organic particles by gas-phase hydroxyl radicals (OH). Laboratory investigations of 50model atmospheric aerosols[2] provide insight into how the formation of new oxygenated 51functional groups (i.e. functionalization) and C-C bond scission (i.e. fragmentation) reactions 52together alter particle composition and size.[3-7] These experimental studies are particularly 53valuable when coupled with detailed kinetics models since the resulting predictive description 54connects key elementary reaction steps to changes in the physical properties of the aerosol.

55

56When an organic aerosol becomes very heavily oxidized, significant concentrations of carboxylic 57acid groups build up on the particle surface.[8] As a result, initially hydrophobic aerosol develops 58hydrophilic character. Under humid conditions, water will accumulate on a hydrophilic surface 59over time, transforming the reaction environment from a purely organic matrix into an aqueous 60solution. This is a very late phase of chemical ageing of a chemical reduced aerosol, and gaining 61an understanding of the factors that control reactivity in this regime and what role may be played 62by carboxylic acid moieties are the primary goals of this work.

63

64There have been a number of important studies of the aqueous phase chemistry of oxidized

65aerosol constituents that examine reaction rates and mechanisms[9-15] as well as the relationship

66between aerosol phase state, heterogeneous reaction rate and ultimately cloud nucleation

67activity.[16-25]   In general these systems exhibit substantial C-C bond fragmentation and

68volatilization, in contrast to what is generally observed in the heterogeneous oxidation of reduced

69organics.[20, 26] For example, levoglucosan, an anhydrosugar, has been widely studied as a model

70for aqueous biomass derived aerosol, undergoes significant fragmentation.[21-22, 27-29] The same

71behavior is reported for the heterogeneous oxidation of aqueous erythritol, another highly

72oxygenated model system.[20, 30] In this case, Kessler et. al.[20] found evidence that hydrogen

73abstraction by OH from a hydroxyl group leads to α-hydroxy alkoxy radical formation and

74subsequent decomposition by C-C bond scission.

75

76The differences in reactivity between heavily and lightly oxidized systems originate from the

77presence of oxygen-containing functional groups located on or adjacent to peroxy and alkoxy

78radical intermediates, whose chemistry in turn controls the extent of fragmentation and

79subsequent volatilization.[20, 31] For example, for a series of structurally related model dicarboxylic

80acid aerosol with a common C_4 backbone, the distribution of primary, secondary and tertiary

81peroxy and alkoxy radicals, formed after the initial OH radical reaction, was observed to play a

82large role in ultimately governing the quantity and identity of smaller molecular weight C-C

83bond scission products.[16-18]   In most of these previous studies experimental observations were

84rationalized solely by free radical reaction pathways initiated by OH. However, we expect that

85for the vast majority of highly oxidized ambient organic aerosol (e.g. secondary organic aerosol),

86which are hydrophilic in nature, the presence of an aqueous phase will lead to carboxylic acids

87being in equilibrium with their conjugate base. Thus, OH will react with both neutral and ionic

88forms. Acid-base chemistry should occur simultaneously with free radical oxidation, and

89constitute an important aging mechanism for particles in the troposphere.

90

91To our knowledge there have been only a few detailed experimental investigations[32-36] of

92heterogeneous OH reactions in systems where free radical and acid-base chemistry can occur

93simultaneously. In this work, we investigate the heterogeneous OH oxidation of aqueous citric

94acid (CA) aerosol by OH. CA is a reasonable model for highly oxidized organic aerosol

95($C_6H_8O_7$), containing three carboxylic acid functional groups and a single alcohol moiety. CA

96should exhibit many of the OH-driven aging pathways that occur in secondary organic aerosol.

97Because of its low pKa, CA is expected to react with OH in both neutral and acid-base forms.

98We develop a molecular level kinetic description of the chemistry for this system using the

99generalized oxidation mechanism for triacontane as a foundation.[8] The model predictions are

100compared to an extensive experimental dataset obtained previously by Davies and Wilson,[37]

101which includes the CA decay kinetics, product mass spectra, elemental ratios, and aerosol size;

102all of which evolve with OH exposure. We focus on the dataset obtained at a relative humidity

103(RH) of 64.5%, where the aerosol is liquid and well-mixed on the timescale of the OH reaction

104frequency. Since the aerosol is an aqueous solution of CA in equilibrium with its conjugate base,

105we have included reactions of OH with ionic species as well as with neutrals. We have performed

106simulations for three scenarios to elucidate how key reaction steps control reactivity and physical

107properties of the aerosol in aqueous vs. non-aqueous aerosol systems. We find that only those

108simulations that include both acid-base and free radical pathways yield model predictions

109consistent with the global experimental dataset.

110

111II.   Model Framework

112Complex sets of chemical reactions are traditionally analyzed using sets of coupled ordinary

113differential equations in which continuous variables evolve deterministically. Although this

114reasonably describes test-tube sized or larger systems,[38] as system size decreases to the size of an

115aerosol, discreteness and stochasticity can have much greater impacts on system behavior. Under

116such conditions, molecular populations are better viewed as integer variables evolving

117stochastically. Kinetiscope©,[39] the software used here, is based on a stochastic algorithm that

118propagates a simulation by randomly selecting among probability-weighted elementary reaction

119steps (events).[40-41] The rate law for each of elementary step is used to calculate the probabilities,

120and establish an absolute time base for direct comparison of simulations to experiment. The

121method has been shown to be a rigorous solution to the master equation for Markov processes. It

122has been extended to simulate kinetics in systems with variable volume[42] and is well suited to

123cases such as aqueous citric acid aerosol oxidation. Additional information is available on the

124software's website and in prior work on aerosol oxidation.[31, 43] Reaction mechanisms are

125constructed inductively, that is, by starting from the simplest description and adding new reaction

126steps when the simulation results fail to agree with experiment. Rate coefficients for each step

127are taken directly from literature, calculated from experimental data or quantum theory, or

128estimated using quantitative structure-activity relationship models. Initial concentrations are used

129to replicate experimental conditions. Further discussion of the methodology is presented in the

130Supplementary Information (SI), section S1.

131

132The current model includes a number of elements previously developed[8, 31, 43] to describe the

133multiphase chemistry of organic aerosols. These elements (outlined briefly in Sec. IIa), include

134the simulation geometry, kinetic descriptions of OH sticking and reaction, evaporation of

135products as well as the central pathways for peroxy and alkoxy reactions. Several new elements,

136outlined in detail in Sec. IIb-d, have been added to simulate the heterogeneous reaction of CA

137aerosol by OH. They include acid-base reactions and equilibria, and accurately capture the

138changes in aerosol size during oxidation due to dynamic uptake and release of ambient water.

139

140*a. OH uptake and reaction, evaporation, and radical reaction pathways*

141*OH uptake*. As described in previous studies, the reaction rate of OH at the surface of the aerosol

142is controlled by two separate elementary steps.[8, 31, 43] First the OH absorbs to a surface site from

143the gas phase, then it reacts with CA or its products. The absorption step is described by a

144pseudo first order rate coefficient (k_{ad} in Table 1). k_{ad} depends on three factors: the OH

145concentration in the gas phase, the gas-surface collision frequency, and the OH sticking

146probability. While two of these are known quantities, the sticking probability is usually not

147known and for this is systems is expected to be rather complex since the aerosol surface has

148substantial water coverage in addition to organic reactants and products.[37] Accordingly, a value

149of 0.052 s^{-1} is determined for k_{ad} by adjusting it until the calculated citric acid concentration vs

150time curve is in quantitative agreement with experiment.[8, 43] The collision frequency of OH, $k_{coll,}$

151at a density of 7.5 x 10^{10} molec/cm^3 with the 10^{-14} cm^2 surface area of the reaction compartment

152(Section IId) is calculated to be 12.4 s^{-1}. Since $k_{ads} = \square k_{coll}$, this gives a value of 4.2 x 10^{-3} for $\square$,

153the sticking coefficient. This is in the range estimated for $\square$ in simulations of OH reacting with

154squalane (10^{-4}) [43] and triacontane (5 x 10^{-5}, calculated from the reported rate coefficient).[8] Since

155the sticking coefficient for water to water surfaces is 1,[44] and OH to water is in the same range,[45]

156the low value suggests that the outer surface of the aerosol has a strongly organic character

157despite the significant amount of water present. All other coefficients in the mechanism are

158derived from experiment and theory.

159

160*Evaporation.* The simulated aerosol volume dynamically evolves both by the formation of higher

161density reaction products that bind water formed by OH reactions or accrete waters of solvation

162from the ambient, and by the evaporation of high volatility small molecule products and

163eventually their water shells. Loss of water is assumed to be instantaneous following desorption

164of products from the aerosol surface. Products containing 2 carbons, such as oxalic acid, have

165much higher vapor pressure than those with 3 carbons and greater,[46] and are assumed to be the

166only ones that undergo significant evaporation. Their vapor pressures are set to be 1 x 10^{-4} Pa, a

167value typical for small dicarboxylic acids at room temperature.[46] The evaporation rate coefficent

168computed from this vapor pressure and the simulation geometry, as described in Wiegel et al, [8, 31]

169is 0.35 s^{-1}.

170

171*Radical reaction pathways.* Because the possible reactions are relatively few, the elementary

172steps used to describe the heterogeneous reaction of CA with OH are written explicitly (i.e.

173involving individual molecules) rather than using the lumped reaction scheme based on

174functional group chemistry introduced previously to model the multi-generational oxidation of

175alkanes.[8, 31] As shown in Table S1 in the SI, the full range of possible reaction products is

176considered and includes C_6 functionalization products as well as C_2-C_5 species formed via C-C

177bond scission reactions. These product species are formed via the generic elementary reaction

178steps, shown in Figure 1, that have been used in previous studies.[4-5, 8, 31, 43, 47-48]

179

180Briefly, OH can abstract a hydrogen atom from a $-CH_2$ or $-OH$ moiety located on CA or its

181reaction products (generically represented as RH in Figure 1). The rate coefficient for H-

182abstraction from these sites are taken from the literature and shown in Table 1. The resulting H-

183abstraction reaction at the $-CH_2$ group produces an alkyl radical (R), which is rapidly converted

184(in the presence of O_2) into a peroxy radical (RO_2). RO_2 is the central intermediate that controls

185much of the oxidative transformation of CA and its subsequent products. For instance, RO_2 +

186RO_2 reactions produce either stable products with new alcohol and carbonyl functionalities or

187alkoxy radicals (RO). Previous work[31] has shown that the aerosol oxidation chemistry is

188consistent with 90% of the secondary RO_2 + RO_2 reactions yielding stable products (i.e. carbonyl

189and alcohol), and the remaining 10% forming alkoxy radicals and O_2. H abstraction from the $-$

190OH group directly forms an alkoxy (RO) radical or, in the case of an -OH group on a carboxylic

191acid, an acyloxy radical. Unimolecular decomposition of alkoxy and acyloxy radicals as well as

192intermolecular H-abstraction by RO are included in the model. As shown in Figure 1,

193hydroperoxide (ROOH) products are formed by the RO_2 + HO_2 reaction.

194

195In following sections, we describe extensions to the oxidation mechanism. They include the

196implementation of the new acid-base reaction steps, the calculation of their rate constants, and a

197description of how these acid-base equilibria are coupled to the free radical reaction scheme

198described above. This is followed by a description of how water is included in the simulation to

199order to properly account for the hygroscopic growth of the aerosol during oxidation.

200

201 *b. Acid-Base chemistry*

202The aqueous environment requires the inclusion of acid-base chemistry in modeling the

203oxidative evolution of the aerosol. While free radical chemistry in hydrophobic organic aerosol is

204well-constrained by known reaction pathways and rate coefficients, little work has explicitly

205focused on how free radical chemistry is modified in aqueous organic aerosol where acid-base

206chemistry occurs simultaneously. CA has a pKa_1 of 3.13, and dissociates in water to produce

207hydronium and citrate, the conjugate base of CA. This relatively acidic environment leads to

208further deprotonation of the numerous triacid and diacid products (see Table S1) formed from

209CA oxidation. Thus, we expect the formation of radical anions as the system is oxidized, and are

210interested in how the reactivity of these radical anions differs from their neutral counterparts (e.g.

211citrate *vs* citric acid). In particular, we focus on the unimolecular fragmentation rates of anionic

212alkoxy radicals compared to their neutral analogs. Because several key rate coefficients have not

213been measured, we used *ab initio* calculations of the reaction barriers to estimate them.

214

215Using Gaussian09,[49] the ground state energy of the radical is obtained by optimization of all its

216conformers using the SMD/IEF-PCM solvent model for water and the M06-2x functional and the

2176-31G(d,p) basis set. The solvent model was shown by Marenich et. al.[50] to reduce mean

218unsigned errors in the solvation energies of both neutral and charged species while the functional

219was shown by Walker et. al.[51] to be a superior choice compared to B3LYP in systems with

220dispersion and ionic hydrogen-bonding interactions. Vibrational frequencies of the ground state

221are computed at the same level of theory to ensure the optimized structure corresponds to a local

222minimum. For the transition state calculation, the Berny option with a calculation of force

223constants is used. The length of the fragmenting C-C bond is set to the value obtained by a

17

9

18

224relaxed potential energy surface scan for a local maximum in total molecular energy. The barrier

225height for dissociation, E_b , is taken as the difference between the ground and transition state

226energies. Rate coefficients for β C-C bond scission of substituted alkoxy radicals are estimated

227using the following structure-activity relationship model developed by Vereecken and Peeters,[52]

228 $$k_{diss}(T)=L \times A_{TST}(298\,K) \times ¿^{\dfrac{\dfrac{T}{298\,K}}{¿}{¿}}$$ (Eq. 1)

229where L is the number of identical bond scissions and $A_{TST}(298\,K)$ is the pre-exponential

230factor at 298 K based on Transition State Theory. Further details are presented in section S5

231of the SI.

232

233As observed in previous work[31, 52-53] and further confirmed by this set of calculations, the barrier

234height for β-scission of an alkoxy radical is found to be lowered when a ketone or hydroxyl

235functional group is located on an adjacent carbon atom as shown in Scheme 1. The reduction in

236barrier height is significant, such that unimolecular decomposition of activated RO is the primary

237sink for alkoxy radicals rather than, for example, hydrogen abstraction (i.e. RO + RH).

238

239 As shown in Scheme 1c, the barrier height for the already-activated alkoxy radical is reduced

240even further when the adjacent carboxyl group is deprotonated. Indeed, $\cdot COOH$ is reported

241to be a fleeting radical while the $\cdot COO^{-¿}_{¿}$ radical anion has been observed to form in aqueous

242solutions due to stabilization by the solvent.[54-57] However, activation of the carboxylate group is

243not limited to those pathways that form $\cdot COO^{-\dot\iota}$. As shown in Scheme 2, formation of a larger

244radical anion is still more favorable than its neutral form. The difference in fragmentation rate

245coefficients calculated using these barriers confirms the necessity of including acid-base
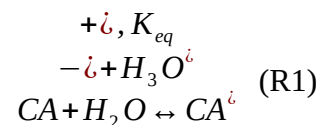
246chemistry in the model to capture the low energy reaction pathways.

247

248*c. Inclusion of rapidly maintained equilibria*.

249Explicit simulations of rapidly maintained acid-base equilibria using stochastic methods are

250exceedingly slow.[39, 58-59] This is because reaction steps at equilibrium have a high probability of

251being selected relative to the other reaction steps, and the simulation's timescale barely advances.

252Thus, explicit inclusion of equilibrium steps for the deprotonation and protonation of carboxyl

253groups in CA is impractical, and they are included implicitly, as described below. Extensive

254checks were made to verify that this approximation does not change the simulation results; they

255are presented in section S3 of the SI.

256

257The deprotonation of CA to form citrate and its subsequent reaction with OH can be described by

258the following steps, where R1 and R2 are added together, and explicit treatment of water and
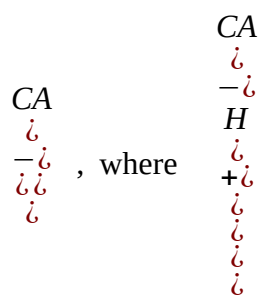
259hydronium formation becomes implicit:

260
$$CA + H_2O \overset{+\dot\iota, K_{eq}}{\underset{}{\leftrightarrow}} CA^{-\dot\iota} + H_3O^{\dot\iota} \quad \text{(R1)}$$

261
$$-\dot{\iota}+H_2O, k_2$$
$$-\dot{\iota}+\cdot OH \rightarrow \cdot CA^{\dot{\iota}}$$
$$CA^{\dot{\iota}}$$
(R2)

262 _____

263
$$+\dot{\iota}, k_3$$
$$-\dot{\iota}+H_3O^{\dot{\iota}}$$
$$CA+\cdot OH \rightarrow \cdot CA^{\dot{\iota}}$$
(R3)

264 The forward rate of reaction ($R3$) $\begin{matrix} CA \\ \dot{\iota} \\ -\dot{\iota} \\ \dot{\iota}\dot{\iota} \\ \dot{\iota} \end{matrix}$, where $\begin{matrix} CA \\ \dot{\iota} \\ -\dot{\iota} \\ H \\ \dot{\iota} \\ +\dot{\iota} \\ \dot{\iota} \\ \dot{\iota} \\ \dot{\iota} \\ \dot{\iota} \end{matrix}$. This yields the rate constant

265 $\begin{matrix} H \\ \dot{\iota} \\ +\dot{\iota} \\ \dot{\iota} \\ \dot{\iota} \end{matrix}$ $k_3 = K_{eq} k_2 \dfrac{[H_2O]}{\dot{\iota}}$. In explicit model runs performed to test this approximation, $\dfrac{[CA]}{\begin{matrix} CA-\dot{\iota} \\ \dot{\iota} \\ \dot{\iota} \end{matrix}}$ has

266 a nearly constant ratio (section S3 in the SI). This justifies the assumption that a strict

267 equilibrium between water and hydronium is maintained, i.e. pH is constant. By using the

268average value of $\dfrac{\overline{\left[H_3O^+\right]}}{\left[H_2O\right]}$ from the explicit model, k_3 is easily computed and is shown in

269Table 1. Thus, $\overline{CA^-}$ is no longer explicitly included in the mechanism, since its concentration

270is embedded in the rate constant k_3 which is proportional to the CA acid-base, K_{eq}. We extend

271this method of modeling protonation and deprotonation to all other acid products in the system

272by using their respective K_a values (Table S1 in the SI), making simulation runtimes much more

273practical.

274

275Some reaction products observed in the experiment contain new carbonyl functionalities. As a

276result, hydration reactions of these species (R=O ↔ R(OH)$_2$) are included in the simulations. The

277equilibrium constants K_h for these products, described below, are computed using structure

278activity relationships in Ref [60] and listed in Table S1 in the SI. In the simulation, hydration is

279assumed to be instantaneous for species with K_h > 100. Otherwise, using the treatment for acid-

280base chemistry described above, K_h is combined with the OH abstraction reaction coefficient for

281the alcohol form (Table 1) to generate an effective rate coefficient.

282

283*d. Treatment of water and aerosol volume.*

284As will be discussed further below, the experimentally observed CA aerosol volume increases by

285~50% during the initial stages of the reaction. In the simulations, the volume is calculated

286dynamically using the instantaneous amounts and densities of all species present (Table S1 in the

287SI). This allows concentrations and reaction rates to be continuously corrected as the volume

288changes.

289

290The substantial volume increase is much larger than can be rationalized solely by the formation

291of oxidation products. Previous studies report a variety of approaches to estimate the

292hygroscopicity of oxidized aerosol, the simplest of which uses O/C as the primary predictor.[61-62]

293Suda et. al.[63] examined the influence of the location and number of functional groups on organic

294aerosol hygroscopicity, and concluded that hydroxylation is a key pathway by which aerosols

295become more hygroscopic. In view of the literature, the likeliest explanation for the initial

296increase in volume is uptake of ambient water, promoted by formation of new hygroscopic

297species during oxidation. After the initial period of growth, the subsequent volume loss

298originates from the desorption of volatile organic compounds and their waters of solvation when

299fragmentation becomes kinetically significant.

300

301In the model described here, the rates of adsorption, absorption and desorption of water

302molecules are assumed to be very fast relative to the chemical reaction rate, and therefore are not

303treated explicitly. Instead, each species in the simulation is assumed always to have a number of

304water molecules solvating it, contributing to its effective density. Because few data are available

305for the size of stable water solvation shells for species involved in the oxidation reactions,

306estimates are made based on the literature value of 6-7 waters per CA molecule, computed for

307neutral species from room temperature solubility data.[64] The average number of waters, 6.5, are

308apportioned among the functionalities as 2 waters per –COOH moiety, and 0.5 waters per alcohol

309 or carbonyl moeity. If a species can deprotonate to form hydronium, the hydronium is modeled

310 as having 3 additional water molecules.[65] We assume that the formation of two adjacent alcohol

311 groups via the hydration of carbonyls results in the addition of 0.5 waters to the solvation shell.

312 Because the model does not explicitly contain ionic species their waters are included indirectly.

313 The percent CA dissociation obtained from explicit model simulations is used as a weighting

314 factor to calculate the average number of water molecules associated with each acidic species.

315 The total number of waters estimated using these criteria for each species is shown in Table S1 in

316 the SI. The partial volume of water is added to the molar volume of the organic to estimate the

317 density of each organic+water group. These values are also listed in Table S1.

318

319 In addition to changes of volume and concentrations in the particle, and thus reaction rates,

320 changes in the surface to volume ratio of the aerosol impact the relative importance of surface

321 and bulk chemical reactions. Because the aqueous aerosol has low viscosity, it is represented

322 using a single instantaneously mixed compartment rather than multiple diffusion-coupled

323 compartments, which has been shown to be valid for reactions in well-mixed aerosol.[31, 43] This is

324 computationally efficient but poses challenges for proper weighting of surface to volume kinetics

325 when there are large volume changes. Bulk reactions occur throughout the volume, but OH

326 adsorption only takes place at the surface. To ensure that this balance is correctly represented in

327 the simulations, the single compartment is treated as a slim 1 nm x 1 nm x $R/3$ nm cuboid in the

328 aerosol, where the outer surface of the aerosol is represented as a fixed 1 nm^2 square and R is the

329 instantaneous radius of the spherical aerosol that is being simulated. This is implemented by

330 assuming that the number of surface sites (1 site per initial surface CA molecule within 1 nm of

331 the surface, calculated from the density of CA in solution), available for adsorption and

332 desorption as the reaction proceeds, is constant. Consequently, the dimension of $R/3$ is equal to

333the ratio of the instantaneous volume to the fixed surface area. This representation maintains the

334correct scaling between compartment volume and area of the spherical aerosol modeled in the

335experiment, and thus the correct weighting of surface and bulk chemical processes.

336

337*e. Photolysis of hydroperoxides*

338There are reaction pathways in the model that produce hydroperoxides (ROOH). As such we

339consider that possibility that if these species are formed that they could be photolyzed by the 254

340nm light source used in the experiment to generate OH. We assume that the photon flux incident

341on particle phase ROOH is the same as that for ozone in the flow tube reactor (value in Table 1).

342The photolysis of ozone can be described as:

343
$$O_3 \xrightarrow{k_p, h\nu} O\left(¿{}^1D\right) + O_2 \left(¿{}^1\Delta\right) ¿ ¿$$
(R4)

344where we determine value of k_p that best replicates the experimental [OH]. A value of

345 $k_p = 0.5 s^{-1}$ produces an average [OH] which matches experiment. From this value, we can

346estimate the rate coefficient for ROOH photolysis by scaling k_p by ratio of ROOH and O_3

347cross sections (σ) at 254 nm and 293.15K,

348
$$ROOH \xrightarrow{} RO\cdot + \cdot OH, k_{photolysis} = \frac{k_p * \sigma_{ROOH}}{\sigma_{ozone}}$$
(R5)

349 σ_{ROOH} is estimated by averaging values for small hydroperoxides CH_3OOH and

350 $HOCH_2OO$ (see Table 1).[66]

351

III.   Results

353The simulation results are compared with previous measurements reported in Davies and 354Wilson.[37] As detailed below, the experimental measurements include: (a) the reactive decay of 355CA, (b) average aerosol elemental composition, product mass spectra and formation kinetics, (c) 356particle volume as a function of OH exposure. A successful model will generate predictions that 357are within the experimental errors for this entire suite of measurements. Three model scenarios 358are considered and compared with experiment in order to explore separately the effects of free 359radical and acid-base chemistry, and to assess the importance of fragment evaporation on the 360physiochemical evolution of the aerosol. As summarized in Table 2, Scenario 1 includes free 361radical chemistry only without evaporation; Scenario 2 includes free radical and acid base 362chemistry without evaporation and Scenario 3, the most complete simulation, includes free 363radical + acid base chemistry and evaporation of C_2 reaction products.

364

a.   Citric Acid Decay as a Function of OH Exposure

366The normalized decay of CA as a function of OH exposure is plotted for the experiment and the 367three model scenarios in Figure 2. All three scenarios accurately predict, within experimental 368error, most of the exponential decay of CA observed in the experiment. The first few 369experimental points at low exposure are the exception: they deviate from a purely exponential 370function. The reason for this is unclear, and is not predicted by any of the model scenarios. 371Phenomenological CA disappearance rate constants (k_{obs}) are extracted from exponential fits to 372the experiment and simulations. As shown in Table 3 the range is relatively small, but Scenario 3 373is in closest agreement with observations.

374

375   *b.   Average Aerosol Elemental Composition and Product Mass Spectra*

376The average aerosol elemental composition observed during the reaction is shown in Figure 3.

377This representation, known as a van Krevelen diagram, shows the relationship between the

378hydrogen-to-carbon (H/C) and oxygen-to-carbon (O/C) ratios. Before reaction the elemental

379composition of CA is H/C = 1.33 and O/C = 1.16. Both the H/C and O/C change substantially

380during the experiment yielding a final average elemental composition of H/C = 1.1 and O/C =

3811.4 at [OH]t = 4.4 x 10^{12} molec. cm^{-3} s. All three scenarios predict similar van Krevelen trends

382and all are within the overall experimental error of the experiment.

383

384Despite similarities in average aerosol composition, significant differences among the scenario

385predictions appear when they are compared to the experimentally observed population of major

386reaction products detected via aerosol mass spectrometry.[37] The ionization source used in the

387experiments is Direct Analysis in Real Time (DART), which produces negatively charged M-H[-]

388ions. For example, neutral CA ($C_6H_8O_7$) molecules appear in the negative ion mass spectrum at

389m/z = 191.02 ($C_6H_7O_7^-$). The experimental data are not corrected for ionization cross section

390differences. Data are shown in Figures 4 and 5.

391

392It is clear from Figure 4 that only Scenario 3 predicts all 5 major products observed aerosol mass

393spectra. There is also good agreement between Scenario 3 and the experimental mass spectrum

394recorded at lower OH exposures (OH exposure = 2.2 x 10^{12} molec. cm^{-3} s) as shown in Figure S5

395in the SI, indicating that this scenario replicates all of the major reaction products observed over

396the course of the reaction. Scenarios 1 and 2 fail to capture the dominant product peak observed

397at m/z = 116.98, which is assigned to mesoxalic acid. Furthermore, Scenario 2 predicts little if

398any m/z = 207.01, assigned to the $C_6H_8O_8$ functionalization product (i.e. CA + an alcohol group).

399Scenario 1 produces only small quantities of the product at m/z = 133.01, assigned to the C_4

400fragmentation product malic acid ($C_4H_6O_5$).

401

402The experimental mesoxalic acid (m/z = 116.98) formation kinetics are compared to predictions

403by the model scenarios in Figure 6. It is clear that while all the scenarios produce some

404mesoxalic acid, since there are multiple pathways for its formation, Scenarios 1 and 2 produce

405mesoxalic acid either too quickly or slowly relative to the experiment. Only Scenario 3 correctly

406predicts the experimentally observed mesoxalic acid formation as a function of OH exposure.

407

408*c. Aerosol volume*

409The measured change in aerosol volume vs. OH exposure is shown in Figure 7. At the start of

410oxidation the aerosol grows by ~50% from the initial unreacted aerosol. As noted above, the

411magnitude of this volume increase cannot be explained solely from a change in density as CA is

412consumed and the reaction products observed in the experimental mass spectrum form (Figure

4134). Rather it is more likely that much of the observed growth is due to an increase in the aerosol

414hygroscopicity (water uptake). The measured aerosol volume reaches a maximum around an OH

415exposure of $\sim 2 \times 10^{12}$ molec. cm^{-3} s after which it decreases towards the end of the reaction, with

416a final volume ~25% larger than the unreacted CA aerosol. It is clear from the experiment that

417there is a complex interplay between the formation and evaporation of reaction products and

418water uptake.

419

420Figure 7 compares experiment with predictions from Scenario 1 (radical only chemistry, no

421evaporation) and Scenario 2 (radical + acid-base chemistry, no evaporation) and Scenario 3

422(radical + acid-base chemistry, with evaporation). Scenario 1 under-predicts the magnitude of

423the change in aerosol volume with OH exposure, while Scenario 2 greatly overestimates the

424change in aerosol volume. Neither Scenario 1 or 2 includes product evaporation, and thus as

425expected cannot capture the decrease in volume at larger OH exposures. In contrast, Scenario 3

426produces the correct shape, within experimental uncertainty, as well as the absolute magnitude of

427the aerosol volume over the entire range of OH exposures used in the experiment.

428
429**IV. Discussion**

430It is clear from Figures 2, 3, 4, 6, and 7 that the Scenario 3 predictions, involving simultaneous

431free radical and acid-base OH oxidation channels with fragmentation and volatilization, correctly

432describe the observed trends in volume, composition and reactivity as a function of OH

433exposure. Comparison of the Scenario predictions reveals that OH-abstraction initiates free

434radical reactions that functionalize the carbon skeleton, while OH reactions with carboxylate

435groups arising from acid-base chemistry activate carbon-carbon bond scission in alkoxy radicals,

436leading to the formation of low molecular weight, highly oxidized products such as malic and

437mesoxalic acid. The extensive fragmentation predicted by Scenarios 2 and 3 is consistent with

438the results of previous studies of oxidation of highly oxidized aerosol as discussed in the

439Introduction, suggesting that carboxylate formation is a key species that drives aerosol

440volatilization. As more highly oxidized products are formed, they accrete water, which causes the

441substantial initial volume growth observed to accompany oxidation. The decrease in volume, at

442larger OH exposures, originates from the formation and subsequent evaporation of volatile C_2

443reaction products along with their waters of solvation into the gas phase, which is held at 62.5%

444RH. These results highlight the significant role of water in controlling not only changes in

445physical properties but also the mechanisms of oxidation and fragmentation of aerosol

446components in the atmosphere.

447

448The importance of including coupled acid-base/free radical reaction pathways is primarily

449revealed by predictions of aerosol composition, since there are no clear features in the CA decay

450kinetics or the average O/C and H/C to indicate that more than free radical chemistry is occurring

451(i.e. all scenario predictions compare favorably with experiment within the error). Rather, a

452primary signature of acid-base chemistry is found in the formation of a specific product:

453mesoxalic acid (m/z = 116.98), which is the most abundant product in CA oxidation. The specific

454reaction channel controlling the formation of this C_3 diacid is the rate at which acyloxy radicals

455form from carboxyl groups. This can occur *via* two distinct pathways: (1) the H atom abstraction

456from a carboxylic acid group by OH and (2) the OH charge transfer reaction at a carboxylate

457group. Figure 8 compares the rate coefficients for these channels, [67-68] showing that *k* for the

458charge transfer pathway is 80 times larger. This explains the simulation predictions using

459Scenario 1, which lacks acid/base chemistry. In Scenario 1, the acyloxy radical formation

460channel, and hence fragmentation, is less important because it is slower than other competing

461hydrogen abstraction reactions (e.g. H atom abstraction from a $-CH_2$ group). The lack of

462carboxylate species in Scenario 1 eliminates the additional carboxylic acid formation pathways

463shown in Figure 9. These pathways, which involve fragmentation and decrease carboxylic acid

464carbons numbers by 1, account for over 90% of the total malonic acid ($C_3H_4O_4$) production in the

465model. As shown in Figure 10, malonic acid is a critical precursor for mesoxalic acid. OH

466radical abstraction from malonic acid followed by O_2 addition forms a peroxy radical which can

467 then react with RO_2 or HO_2 to yield mesoxalic acid. The simulations suggest that the RO_2 and

468 HO_2 pathways to form mesoxalic acid are equally important.

469

470 The decarboxylation pathway (Figure 9), is operative only in those Scenarios that include acid

471 -base chemistry (Scenarios 2 and 3) and is the major source of C_3 products generated by CO_2

472 elimination from C_4 species. This is clearly seen in the carbon number plot in Figure 11, where

473 Scenario 1 produces mainly C_4 products and only very small quantities of C_3 reaction products,

474 unlike Scenarios 2 and 3 (which include carboxylate pathways) and the experimental

475 observations.

476

477 As seen in Figure 11, another notable difference between Scenario 1 and Scenarios 2 and 3 is the

478 production rate of C_5 products, which are observed in the experiments. This result can be

479 explained by the relative barrier heights for alkoxy radical decomposition. As shown in Figure

480 12, H atom abstraction by OH from the alcohol group of CA forms an alkoxy radical adjacent to

481 a carboxyl functionality. The subsequent unimolecular fragmentation rate of the alkoxy radical

482 anion in aqueous solution is many orders of magnitude faster than that of its neutral form,

483 particularly if a carboxylate forms during the C-C bond rupture. Accordingly, the resulting C_5

484 product, β-ketoglutaric acid ($C_5H_6O_5$), which is observed experimentally is only produced in

485 Scenarios 2 and 3 (Figure 11) via reaction pathways involving the conjugate base of CA. When

486 acid-base chemistry is absent (i.e. Scenario 1) this particular fragmentation pathway is of minor

487 importance because it is slow relative to other possible alkoxy radical reactions. Interestingly, the

488 differences in product distributions due to the presence or absence of acid-base chemistry have a

489 negligible impact on the predicted van Krevelen diagrams. This suggests that average aerosol

490elemental composition, not surprisingly, is a blunt probe of the underlying elementary reaction

491pathways.

492

493The acyloxy reaction pathway shown in Figure 9 is the direct route to transform mesoxalic acid

494into oxalic acid. Oxalic acid, the most abundant atmospheric particulate organic diacid, has

495temporally varying concentrations (seasonal and diurnal) that suggest its abundance is controlled

496by secondary processes.[69-72] Indeed, field measurements of oxalic acid support an in-cloud

497formation mechanism.[73-74] In model scenarios 2 and 3, oxalic acid is the most abundant acid in

498the system by the end of the simulation runs. Thus, the activation of the carboxylate group

499towards acyloxy radical formation and its subsequent reactions as shown in Figures 8 and 9

500provide a possible mechanism for oxalic acid formation in the atmosphere.

501

502The aerosol volumes (Figure 7) predicted in Scenarios 1 and 2 continuously increase over time,

503in contrast to Scenario 3 (and the experiment), which exhibit a maximum. This is not surprising

504since only Scenario 3 allows for the production of reaction products that partition to the gas

505phase resulting in a net decrease of material in the aerosol. In particular, we find that C_2 product

506evaporation is the most important contributor to the observed decrease in aerosol volume. The

507large increase in aerosol volume at early OH exposures can be explained by an increase of

508aerosol hygroscopicity due to the increase in the total quantity of soluble molecules (i.e.

509fragmentation products) originating from the extensive C-C bond scission chemistry discussed

510above. This initial increase is much steeper for Scenario 2 than 1 and can be explained by the

511larger population of C_3 and C_5 fragmentation products (Figure 11) produced in Scenario 2 via the

512carboxylate reactions discussed above.

513

514Finally, in all three scenarios, ROOH photolysis is found to be a negligible reaction pathway. In

515the simulations, photolysis occurs on average once for every 20,000 β-scission reactions. Rather,

516the main sink for ROOH is C-H attack by OH, as shown in Figure 13, which functionalizes the

517carbon skeleton with a ketone group. Subsequent hydration, hydrogen abstraction from the

518hydroxyl group, and fragmentation yields oxaloacetic acid ($C_4H_4O_5$), the key C_4 product

519undergoing the carboxyl-forming pathway in Figure 9. Thus, ketone production from ROOH

520reaction with OH is a major contributor to eventual C_3 product formation. This is only possible

521when acid-base chemistry activates acyloxy radical formation.

522

523**V. Conclusion**

524A detailed, physically based kinetics model is formulated for the heterogeneous oxidation of

525aqueous citric acid aerosol by OH. Citric acid is a reasonable proxy for understanding the

526fundamental chemical pathways that might be important for prediction of secondary organic

527aerosol and late-stage aging of primary aerosol in the troposphere. We find that substantial

528coupling of acid-base and free radical chemistry is needed to explain the heterogeneous

529oxidation of CA by OH, and that carboxylate groups are central to trends in aerosol composition

530and size observed as a function of OH exposure. When present in carboxylic acid form only,

531reactions with OH lead mainly to functionalization of CA. When neutral CA is equilibrated with

532its conjugate base, extensive fragmentation occurs following H abstraction. Larger carbon

533numbered diacids are transformed into smaller diacids through the interplay of acid-base and free

534radical chemistry, activating acyloxy formation and driving subsequent decarboxylation and

535carboxyl-group formation. In addition, the carboxylate group significantly lowers the barrier

536height to C-C bond scission in alkoxy radicals. Together, these two effects of acid-base chemistry

537are essential to simultaneously predict the kinetic decay of citric acid, changes in aerosol volume,

538and the product distribution within the aerosol. The presence of mesoxalic acid as a product is a

539key signature of acid-base chemistry in this system; reaction rates and elemental compositions

540alone do not provide evidence that this reaction channel is occurring. The simulation results also

541provide insight to how elementary reaction steps controls the evolution of aerosol size during

542oxidation. The detailed trend is controlled by a subtle balance of chemical erosion and

543hygroscopic growth.

544

545How does this fit in with what is known about aerosol ageing processes? As shown by Lambe et

546al.,[75] the quantity of secondary aerosol formed by the reaction of OH with alkanes evolves

547dynamically by functionalization and fragmentation.[3] Functionalization dominates early stage

548oxidation and leads to substantial aerosol yield. At higher oxidation levels, the aerosol yield

549reaches a maximum, and further reaction reduces the quantity of aerosol by the production of gas

550phase products (i.e. fragmentation). Carboxylic acids are expected to be key particle phase

551products that contribute substantially to lowering aerosol volatility (i.e. enhancing the quantity of

552aerosol) while   raising its oxidation state and hygroscopicity.   Our results suggest a new

553connection between aerosol pH and water that may govern the balance of functionalization and

554fragmentation in aqueous secondary organic aerosol.   As the oxidation state of the aerosol

555increases by the formation of acids, water uptake naturally follows, opening acid-base reaction

556channels. This indicates that carboxylic acids could play a dual role. At early stages, these highly

557oxidized species mainly contribute to increase in aerosol mass and water uptake. When the

558character of the aerosol becomes aqueous, acid-base equilibria lead to an increase in carboxylate-

559mediated chemistry which largely consists of C-C bond scission reactions (i.e. chemical erosion).

560

561Here we have considered only a single relative humidity (RH = 64.5%) where the aerosol is a

562well-mixed aqueous solution on the timescale of the OH reaction frequency. We expect more

563complex behavior to appear as the RH is lowered and the aerosol and its subsequent

564transformations are governed increasingly by nanoscale interfacial gradients produced by slow

565diffusional timescales in the particle.[8, 37] For these cases we might expect much more complex

566feedbacks to emerge between aerosol viscosity and hygroscopicity and the underlying

567elementary free radical and acid-base reaction pathways.

568

569**Supporting Information**

570Model construction; Structures, pKa, Kh and densities of organic acid species used in

571simulations;   Validation of implicit acid-base modeling (explicit acid-base model results);

572Comparison of scenario 3 mass spectrum with experiment; Sample Gaussian09 results for alkoxy

573radical anion ground state and transition state; Evaluation of sensitivity of the simulation results

574for Scenario 3 with faster peroxy-peroxy kinetics

575

576**Acknowledgements**

592

593**References**
594

5951.	Buseck, P. R.; Pósfai, M., Airborne minerals and related aerosol particles: Effects on
596climate and the environment. *Proceedings of the National Academy of Sciences of the United
597States of America* **1999,** *96*, 3372-3379.

5982.	Burkholder, J.; Abbatt, J.; Barnes, I.; Roberts, J.; Melamed, M.; Ammann, M.; Bertram,
599A.; Cappa, C.; Carlton, A. M.; Carpenter, L. J., The essential role for laboratory studies in
600atmospheric chemistry. *Environmental Science and Technology* **2017**.

6013.	Kroll, J. H.; Smith, J. D.; Che, D. L.; Kessler, S. H.; Worsnop, D. R.; Wilson, K. R.,
602Measurement of fragmentation and functionalization pathways in the heterogeneous oxidation of
603oxidized organic aerosol. *Physical Chemistry Chemical Physics* **2009,** *11*, 8005-8014.

6044.	George, I. J.; Abbatt, J. P. D., Heterogeneous oxidation of atmospheric aerosol particles
605by gas-phase radicals. *Nature chemistry* **2010,** *2*, 713-722.

6065.	George, I. J.; Slowik, J.; Abbatt, J. P. D., Chemical aging of ambient organic aerosol from
607heterogeneous reaction with hydroxyl radicals. *Geophysical Research Letters* **2008,** *35*.

6086.	Kolesar, K. R.; Buffaloe, G.; Wilson, K. R.; Cappa, C. D., OH-initiated heterogeneous
609oxidation of internally-mixed squalane and secondary organic aerosol. *Environmental Science
610and Technology* **2014,** *48*, 3196-3202.

6117.   Nah, T.; Kessler, S. H.; Daumit, K. E.; Kroll, J. H.; Leone, S. R.; Wilson, K. R., OH-
612initiated oxidation of sub-micron unsaturated fatty acid particles. *Physical Chemistry Chemical*
613*Physics* **2013,** *15*, 18649-63.

6148.   Wiegel, A. A.; Liu, M.; Hinsberg, W. D.; Wilson, K. R.; Houle, F. A., Diffusive
615confinement of free radical intermediates in the OH radical oxidation of semisolid aerosol.
616*Physical Chemistry Chemical Physics* **2017,** *19*, 6814-6830.

6179.   Herrmann, H., Kinetics of aqueous phase reactions relevant for atmospheric chemistry.
618*Chemical Reviews* **2003,** *103*, 4691-4716.

61910.   Herrmann, H.; Schaefer, T.; Tilgner, A.; Styler, S. A.; Weller, C.; Teich, M.; Otto, T.,
620Tropospheric aqueous-phase chemistry: kinetics, mechanisms, and its coupling to a changing gas
621phase. *Chemical Reviews* **2015,** *115*, 4259-4334.

62211.   Blando, J. D.; Turpin, B. J., Secondary organic aerosol formation in cloud and fog
623droplets: A literature evaluation of plausibility. *Atmospheric Environment* **2000,** *34*, 1623-1632.

62412.   Ervens, B.; Feingold, G.; Frost, G. J.; Kreidenweis, S. M., A modeling of study of
625aqueous production of dicarboxylic acids: 1. Chemical pathways and speciated organic mass
626production. *Journal of Geophysical Research D: Atmospheres* **2004,** *109*, 1-20.

62713.   Marais, E. A.; Jacob, D. J.; Jimenez, J. L.; Campuzano-Jost, P.; Day, D. A.; Hu, W.;
628Krechmer, J.; Zhu, L.; Kim, P. S.; Miller, C. C.; etal, Aqueous-phase mechanism for secondary
629organic aerosol formation from isoprene: application to the southeast United States and co-
630benefit of SO_2 emission controls. *Atmos. Chem. Phys.* **2016,** *16*, 1603-1618.

63114.   Lim, Y. B.; Tan, Y.; Perri, M. J.; Seitzinger, S. P.; Turpin, B. J., Aqueous chemistry and its
632role in secondary organic aerosol (SOA) formation. *Atmos. Chem. Phys.* **2010,** *10*, 10521-10539.

63315.   Schone, L.; Schindelka, J.; Szeremeta, E.; Schaefer, T.; Hoffmann, D.; Rudzinski, K. J.;
634Szmigielski, R.; Herrmann, H., Atmospheric aqueous phase radical chemistry of the isoprene
635oxidation products methacrolein, methyl vinyl ketone, methacrylic acid and acrylic acid -
636kinetics and product studies. *Physical Chemistry Chemical Physics* **2014,** *16*, 6257-6272.

63716.   Chan, M. N.; Zhang, H. F.; Goldstein, A. H.; Wilson, K. R., Role of water and phase in
638the heterogeneous oxidation of solid and aqueous succinic acid aerosol by hydroxyl radicals.
639*Journal of Physical Chemistry C* **2014,** *118*, 28978-28992.

64017.   Cheng, C. T.; Chan, M. N.; Wilson, K. R., The role of alkoxy radicals in the
641heterogeneous reaction of two structural isomers of dimethylsuccinic acid. *Physical Chemistry*
642*Chemical Physics* **2015,** *17*, 25309-25321.

64318.   Cheng, C. T.; Chan, M. N.; Wilson, K. R., Importance of unimolecular HO_2 elimination
644in the heterogeneous OH reaction of highly oxygenated tartaric acid aerosol. *Journal of Physical*
645*Chemistry A* **2016,** *120*, 5887-5896.

55

56

64619. Kessler, S. H.; Nah, T.; Daumit, K. E.; Smith, J. D.; Leone, S. R.; Kolb, C. E.; Worsnop,
647D. R.; Wilson, K. R.; Kroll, J. H., OH-initiated heterogeneous aging of highly oxidized organic
648aerosol. *Journal of Physical Chemistry A* **2012,** *116*, 6358-6365.

64920. Kessler, S. H.; Smith, J. D.; Che, D. L.; Worsnop, D. R.; Wilson, K. R.; Kroll, J. H.,
650Chemical sinks of organic aerosol: Kinetics and products of the heterogeneous oxidation of
651erythritol and levoglucosan. *Environmental Science and Technology* **2010,** *44*, 7005-7010.

65221. Slade, J. H.; Knopf, D. A., Heterogeneous OH oxidation of biomass burning organic
653aerosol surrogate compounds: assessment of volatilisation products and the role of OH
654concentration on the reactive uptake kinetics. *Physical Chemistry Chemical Physics* **2013,** *15*,
6555898-915.

65622. Slade, J. H.; Knopf, D. A., Multiphase OH oxidation kinetics of organic aerosol: The role
657of particle phase state and relative humidity. *Geophysical Research Letters* **2014,** *41*, 5297-5306.

65823. Slade, J. H.; Shiraiwa, M.; Arangio, A.; Su, H.; Pöschl, U.; Wang, J.; Knopf, D. A., Cloud
659droplet activation through oxidation of organic aerosol influenced by temperature and particle
660phase state. *Geophysical Research Letters* **2017,** *44*, 1583-1591.

66124. Harmon, C. W.; Ruehl, C. R.; Cappa, C. D.; Wilson, K. R., A statistical description of the
662evolution of cloud condensation nuclei activity during the heterogeneous oxidation of squalane
663and bis(2-ethylhexyl) sebacate aerosol by hydroxyl radicals. *Physical Chemistry Chemical*
664*Physics* **2013,** *15*, 9679-9693.

66525. George, I.; Chang, R.-W.; Danov, V.; Vlasenko, A.; Abbatt, J., Modification of cloud
666condensation nucleus activity of organic aerosols by hydroxyl radical heterogeneous oxidation.
667*Atmospheric Environment* **2009,** *43*, 5038-5045.

66826. Kroll, J. H.; Donahue, N. M.; Jimenez, J. L.; Kessler, S. H.; Canagaratna, M. R.; Wilson,
669K. R.; Altieri, K. E.; Mazzoleni, L. R.; Wozniak, A. S.; Bluhm, H.; etal, Carbon oxidation state as
670a metric for describing the chemistry of atmospheric organic aerosol. *Nature Chemistry* **2011,** *3*
671(2), 133-139.

67227. Hoffmann, D.; Tilgner, A.; Iinuma, Y.; Herrmann, H., Atmospheric stability of
673levoglucosan: a detailed laboratory and modeling study. *Environmental Science & Technology*
674**2010,** *44*, 694-699.

67528. Zhao, R.; Mungall, E. L.; Lee, A. K. Y.; Aljawhary, D.; Abbatt, J. P. D., Aqueous-phase
676photooxidation of levoglucosan-A mechanistic study using aerosol time-of-flight chemical
677ionization mass spectrometry (Aerosol ToF-CIMS). *Atmospheric Chemistry and Physics* **2014,**
678*14*, 9695-9705.

67929. Hennigan, C. J.; Sullivan, A. P.; Collett, J. L.; Robinson, A. L., Levoglucosan stability in
680biomass burning particles exposed to hydroxyl radicals. *Geophysical Research Letters* **2010,** *37*,
681L09806.

68230.   Daumit, K. E.; Carrasquillo, A. J.; Hunter, J. F.; Kroll, J. H., Laboratory studies of the 683aqueous-phase oxidation of polyols: Submicron particles vs. bulk aqueous solution. *Atmospheric* 684*Chemistry and Physics* **2014,** *14,* 10773-10784.

68531.   Wiegel, A. A.; Wilson, K. R.; Hinsberg, W. D.; Houle, F. A., Stochastic methods for 686aerosol chemistry: a compact molecular description of functionalization and fragmentation in the 687heterogeneous oxidation of squalane aerosol by OH radicals. *Physical Chemistry Chemical* 688*Physics* **2015,** *17,* 4398-4411.

68932.   Enami, S.; Hoffmann, M. R.; Colussi, A. J., In situ mass spectrometric detection of 690interfacial intermediates in the oxidation of RCOOH(aq) by gas-phase OH-radicals. *Journal of* 691*Physical Chemistry A* **2014,** *118* (23), 4130-4137.

69233.   Enami, S.; Hoffmann, M. R.; Colussi, A. J., OH-radical specific addition to glutathione S-693atom at the air-water interface: relevance to the redox balance of the lung epithelial lining fluid. 694*Journal of Physical Chemistry Letters* **2015,** *6* (19), 3935-3943.

69534.   Enami, S.; Hoffmann, M. R.; Colussi, A. J., Stepwise oxidation of aqueous dicarboxylic 696acids by gas-phase OH radicals. *Journal of Physical Chemistry Letters* **2015,** *6* (3), 527-534.

69735.   Enami, S.; Sakamoto, Y., OH-radical oxidation of surface-active cis-pinonic acid at the 698air-water interface. *Journal of Physical Chemistry A* **2016,** *120* (20), 3578-3587.

69936.   Kameel, F. R.; Riboni, F.; Hoffmann, M. R.; Enami, S.; Colussi, A. J., Fenton oxidation 700of gaseous isoprene on aqueous surfaces. *Journal of Physical Chemistry C* **2014,** *118* (50), 70129151-29158.

70237.   Davies, J. F.; Wilson, K. R., Nanoscale interfacial gradients formed by the reactive uptake 703of OH radicals onto viscous aerosol surfaces. *Chem. Sci.* **2015,** *6,* 7020-7027.

70438.   Gillespie, D. T., Stochastic simulation of chemical kinetics. *Annual Review of Physical* 705*Chemistry* **2007,** *58,* 35-55.

70639.   Hinsberg, W. D.; Houle, F. A., *Kinetiscope*. Columbia Hill Technical Consulting: 707Fremont, CA: www.hinsberg.net/kinetiscope, 2015.

70840.   Bunker, D. L.; Garrett, B.; Kleindienst, T.; Long, G. S., Discrete simulation methods in 709combustion kinetics. *Combust Flame* **1974,** *23* (3), 373-379.

71041.   Gillespie, D. T., General method for numerically simulating stochastic time evolution of 711coupled chemical reactions. *J Comput Phys* **1976,** *22* (4), 403-434.

71242.   Wallraff, G.; Hutchinson, J.; Hinsberg, W.; Houle, F.; Seidel, P.; Johnson, R.; Oldham, 713W., Thermal and acid-catalyzed deprotection kinetics in candidate deep-ultraviolet resist 714materials. *J Vac Sci Technol B* **1994,** *12* (6), 3857-3862.

71543.   Houle, F. A.; Hinsberg, W. D.; Wilson, K. R., Oxidation of a model alkane aerosol by OH
716radical: the emergent nature of reactive uptake. *Physical Chemistry Chemical Physics* **2015,** *17,*
7174412-4423.

71844.   Davidovits, P.; Worsnop, D. R.; Jayne, J. T.; Kolb, C. E.; Winkler, P.; Vrtala, A.; Wagner,
719P. E.; Kulmala, M.; Lehtinen, K. E. J.; Vesala, T.; Mozurkewich, M., Mass accommodation
720coefficient of water vapor on liquid water. *Geophysical Research Letters* **2004,** *31* (22).

72145.   Garrett, B. C.; Schenter, G. K.; Morita, A., Molecular simulations of the transport of
722molecules across the liquid/vapor interface of water. *Chemical Reviews* **2006,** *106* (4), 1355-
7231374.

72446.   Soonsin, V.; Zardini, A. A.; Marcolli, C.; Zuend, A.; Krieger, U. K., The vapor pressures
725and activities of dicarboxylic acids reconsidered: the impact of the physical state of the aerosol.
726*Atmospheric Chemistry and Physics* **2010,** *10,* 11753-11767.

72747.   Hearn, J. D.; Renbaum, L. H.; Wang, X.; Smith, G. D., Kinetics and products from
728reaction of Cl radicals with dioctyl sebacate (DOS) particles in O2: a model for radical-initiated
729oxidation of organic aerosols. *Physical Chemistry Chemical Physics* **2007,** *9,* 4803-4813.

73048.   Renbaum, L. H.; Smith, G. D., The importance of phase in the radical-initiated oxidation
731of model organic aerosols: reactions of solid and liquid brassidic acid particles. *Physical*
732*Chemistry Chemical Physics* **2009,** *11,* 2441-2451.

73349.   Frisch, M. J. T., G. W.; Schlegel, H. B.; Scuseria, G. E.; Robb, M. A.; Cheeseman, J. R.;
734Scalmani, G.; Barone, V.; Mennucci, B.; Petersson, G. A.; Nakatsuji, H.; Caricato, M.; Li, X.;
735Hratchian, H. P.; Izmaylov, A. F.; Bloino, J.; Zheng, G.; Sonnenb, D. J., *Gaussian09.* Gaussian,
736Inc.: Wallingford, CT, 2009.

73750.   Marenich, A. V.; Cramer, C. J.; Truhlar, D. G., Universal solvation model based on solute
738electron density and on a continuum model of the solvent defined by the bulk dielectric constant
739and atomic surface tensions. *Journal of Physical Chemistry B* **2009,** *113,* 6378-6396.

74051.   Walker, M.; Harvey, A. J. A.; Sen, A.; Dessent, C. E. H., Performance of M06, M06-2X,
741and M06-HF density functionals for conformationally flexible anionic clusters: M06 functionals
742perform better than B3LYP for a model system with dispersion and ionic hydrogen-bonding
743interactions. *Journal of Physical Chemistry A* **2013,** *117,* 12590-12600.

74452.   Vereecken, L.; Peeters, J., Decomposition of substituted alkoxy radicals--part I: a
745generalized structure-activity relationship for reaction barrier heights. *Physical Chemistry*
746*Chemical Physics* **2009,** *11,* 9062-9074.

74753.   Nah, T.; Zhang, H.; Worton, D. R.; Ruehl, C. R.; Kirk, B. B.; Goldstein, A. H.; Leone, S.
748R.; Wilson, K. R., Isomeric product detection in the heterogeneous reaction of hydroxyl radicals
749with aerosol composed of branched and linear unsaturated organic molecules. *The Journal of*
750*Physical Chemistry A* **2014,** *118,* 11555-11571.

75154.   Francisco, J. S. M., James T.; Yu, Hua-Gen, HOCO radical chemistry. *Accounts of*
752*Chemical Research* **2010,** *43*, 1519-1526.

75355.   Hart, E. J.; Henglein, A., Free radical and free atom reactions in the sonolysis of aqueous
754iodide and formate solutions. *The Journal of Physical Chemistry* **1985,** *89*, 4342-4347.

75556.   Janik, I.; Tripathi, G. N. R., The nature of the superoxide radical anion in water. *Journal*
756*of Chemical Physics* **2013,** *139*, 014302.

75757.   Milligan, D. E.; Jacox, M. E., Infrared spectrum and structure of intermediates in the
758reaction of OH with CO. *Journal of Chemical Physics* **1971,** *54*, 927-942.

75958.   Hinsberg, W.; Houle, F. A., Stochastic simulation method for processes containing
760equilibrium steps. *U. S. Patent No. 5625579 (April 29)* **1997**.

76159.   Rathinam, M.; Petzold, L. R.; Cao, Y.; Gillespie, D. T., Stiffness in stochastic chemically
762reacting systems: The implicit tau-leaping method. *Journal of Chemical Physics* **2003,** *119*,
76312784-12794.

76460.   Raventos-Duran, T.; Camredon, M.; Valorso, R.; Mouchel-Vallon, C.; Aumont, B.,
765Structure-activity relationships to estimate the effective Henry's law constants of organics of
766atmospheric interest. *Atmos. Chem. Phys.* **2010,** *10* (16), 7643-7654.

76761.   Lambe, A. T.; Onasch, T. B.; Massoli, P.; Croasdale, D. R.; Wright, J. P.; Ahern, A. T.;
768Williams, L. R.; Worsnop, D. R.; Brune, W. H.; Davidovits, P., Laboratory studies of the
769chemical composition and cloud condensation nuclei (CCN) activity of secondary organic
770aerosol (SOA) and oxidized primary organic aerosol (OPOA). *Atmospheric Chemistry and*
771*Physics* **2011,** *11*, 8913-8928.

77262.   Massoli, P.; Lambe, A. T.; Ahern, A. T.; Williams, L. R.; Ehn, M.; Mikkilä, J.;
773Canagaratna, M. R.; Brune, W. H.; Onasch, T. B.; Jayne, J. T.; etal, Relationship between aerosol
774oxidation level and hygroscopic properties of laboratory generated secondary organic aerosol
775(SOA) particles. *Geophysical Research Letters* **2010,** *37*, 1-5.

77663.   Suda, S. R.; Petters, M. D.; Yeh, K.; Strollo, C.; Matsunaga, A.; Faulhaber, A.; Ziemann,
777P. J.; Prenni, A. J.; Carrico, C. M.; Sullivan, R. C.; etal, Influence of functional groups on organic
778aerosol cloud condensation nucleus activity. *Environmental science & technology* **2014,** *48*,
77910182-90.

78064.   Peng, C. G.; Chow, A. H. L.; Chan, C. K., Hygroscopic study of glucose, citric acid, and
781sorbitol using an electrodynamic balance: Comparison with UNIFAC predictions. *Aerosol Sci*
782*Tech* **2001,** *35*, 753-758.

78365.   Swanson, J. M. J.; Maupin, C. M.; Chen, H.; Petersen, M. K.; Xu, J.; Wu, Y.; Voth, G. A.,
784Proton solvation and transport in aqueous and biomolecular systems: insights from computer
785simulations. *The Journal of Physical Chemistry B* **2007,** *111*, 4300-4314.

78666.   Sander, S. P.; Ravishankara, A. R.; Golden, D. M.; Kolb, C. E.; Kurylo, M. J.; Molina, M.
787J.; Moortgat, G. K.; Finlayson-Pitts, B. J., Chemical kinetics and photochemical data for use in
788atmospheric studies: evaluation number 14. *JPL Publication 02-25* **2003,** *14*, 1-334.

78967.   Buxton, G. V.; Greenstock, C. L.; Helman, W. P.; Ross, A. B., Critical Review of rate
790constants for reactions of hydrated electrons, hydrogen atoms and hydroxyl radicals (.OH/.O-) in
791Aqueous Solution. *Journal of Physical and Chemical Reference Data* **1988,** *17*, 513-886.

79268.   Doussin, J. F.; Monod, A., Structure-activity relationship for the estimation of OH-
793oxidation rate constants of carbonyl compounds in the aqueous phase. *Atmospheric Chemistry
794and Physics Discussions* **2013,** *13*, 15949-15991.

79569.   Kawamura, K.; Kasukabe, H.; Barrie, L. A., Source and reaction pathways of
796dicarboxylic acids, ketoacids and dicarbonyls in arctic aerosols: One year of observations.
797*Atmospheric Environment* **1996,** *30*, 1709-1722.

79870.   Kawamura, K.; Yasui, O., Diurnal changes in the distribution of dicarboxylic acids,
799ketocarboxylic acids and dicarbonyls in the urban Tokyo atmosphere. *Atmospheric Environment*
800**2005,** *39*, 1945-1960.

80171.   Mochida, M.; Umemoto, N.; Kawamura, K.; Uematsu, M., Bimodal size distribution of
802C-2-C-4 dicarboxylic acids in the marine aerosols. *Geophysical Research Letters* **2003,** *30*, 1672.

80372.   Rogge, W. F.; Mazurek, M. A.; Hildemann, L. M.; Cass, G. R.; Simoneit, B. R. T.,
804Quantification of urban organic aerosols at a molecular level: Identification, abundance and
805seasonal variation. *Atmospheric Environment Part A, General Topics* **1993,** *27*, 1309-1330.

80673.   Crahan, K. K.; Hegg, D.; Covert, D. S.; Jonsson, H., An exploration of aqueous oxalic
807acid production in the coastal marine atmosphere. *Atmospheric Environment* **2004,** *38*, 3757-
8083764.

80974.   Yu, J. Z.; Huang, X.-F.; Xu, J.; Hu, M., When aerosol sulfate goes up, so does oxalate:
810implication for the formation mechanisms of oxalate. *Environmental science & technology* **2005,**
811*39*, 128-133.

81275.   Lambe, A. T.; Onasch, T. B.; Croasdale, D. R.; Wright, J. P.; Martin, A. T.; Franklin, J. P.;
813Massoli, P.; Kroll, J. H.; Canagaratna, M. R.; Brune, W. H. e. a., Transitions from
814functionalization to fragmentation reactions of laboratory secondary organic aerosol (SOA)
815generated from the OH oxidation of alkane precursors. *Environmental Science & Technology*
816**2012,** *46*, 5430-5437.

81776.   Denisov, E. T.; Afanas'ev, I. B., *Oxidation and Antioxidants in Organic Chemistry and
818Biology*. Taylor & Francis: Boca Raton, FL, 2005.

81977.   Sander, R., Compilation of Henry's law constants (version 4.0) for water as solvent.
820*Atmos. Chem. Phys.* **2015,** *15*, 4399-4981.

82178.   Doussin, J. F.; Monod, A., Structure–activity relationship for the estimation of OH-
822oxidation rate constants of carbonyl compounds in the aqueous phase. *Atmos. Chem. Phys.* **2013,**
823*13*, 11625-11641.

82479.   Monod, A.; Doussin, J. F., Structure-activity relationship for the estimation of OH-
825oxidation rate constants of aliphatic organic compounds in the aqueous phase: alkanes, alcohols,
826organic acids and bases. *Atmospheric Environment* **2008,** *42*, 7611-7622.

82780.   Sander, S. P. G., D. M.; Kurylo, M. J.; Moortgat, G. K.; Wine, P. H.; Ravishankara, A. R.;
828Kolb, C. E.; Molina, M. J.; Finlayson-Pitts, B. J.; Huie, R. E.; et al, Chemical kinetics and
829photochemical data for use in atmospheric studies evaluation number 15. *JPL Publication 06-2*
830**2006,** *15*, 1-523.

83181.   Atkinson, R.; Baulch, D. L.; Cox, R. A.; Crowley, J. N.; Hampson, R. F.; Hynes, R. G.;
832Jenkin, M. E.; Rossi, M. J.; Troe, J., Evaluated kinetic and photochemical data for atmospheric
833chemistry: Volume I - gas phase reactions of Ox, HOx, NOx and SOx species. *Atmos. Chem.*
834*Phys.* **2004,** *4*, 1461-1738.

83582.   Wallington, T. J.; Dagaut, P.; Kurylo, M. J., UV absorption cross sections and reaction
836kinetics and mechanisms for peroxy radicals in the gas phase. *Chemical Reviews* **1992,** *92*, 667-
837710.

83883.   Vaghjiani, G. L.; Ravishankara, A. R., Kinetics and mechanism of hydroxyl radical
839reaction with methyl hydroperoxide. *The Journal of Physical Chemistry* **1989,** *93*, 1948-1959.

840

841
842

843

Table 1: Key Model Parameters and Rate Coefficients

844**Table 1: Key Model Parameters and Rate Coefficients**

845

Parameter	Value	Description and References
RH	64.5%	Relative Humidity
d_p	97 nm	Diameter of particle
k_{ad}	0.052 s^{-1}	Pseudo-first order adsorption rate coefficient of OH
[OH]	7.5×10^{10} molec. cm^{-3}	Average experimental [OH][37]
k_{RO2+O2}	2.0×10^5 s^{-1}	Pseudo-first order reaction rate coefficient of $RO_2 + O_2$[a]
$k_{photolysis}$	1.3×10^{-4} s^{-1}	Rate coefficient of ROOH photolysis (see text for details)
$k_{CA(CH2)+OH}$	5.1×10^{-14} cm^3 molecules^{-1} s^{-1}	Rate coefficient of H abstraction from -CH$_2$ group in CA [b]
$k_{CA(OH)+OH}$	9.7×10^{-14} cm^3 molecules^{-1} s^{-1}	Rate coefficient of H abstraction from -OH group in CA[b]
$k_{RO2+HO2}$	3.8×10^{-15} cm^3 molecules^{-1} s^{-1}	Rate coefficient of $RO_2 + HO_2$ [c]
$k_{ROOH+OH}$	3.7×10^{-12} cm^3 molecules^{-1} s^{-1}	Rate coefficient of ROOH + OH[d]
$k_{RO2+RO2}$	1.6×10^{-15} cm^3 molecules^{-1} s^{-1}	Rate coefficient of $RO_2 + RO_2$ [76]
$k_{RCOOH+OH}$	2.3×10^{-15} cm^3 molecules^{-1} s^{-1}	Rate coefficient of RCOOH + OH [e, 67]
$k_{RCOO-+OH}$	2.0×10^{-13} cm^3 molecules^{-1} s^{-1}	Rate coefficient of RCOO- + OH[68]
k_{HO2+OH}	1.7×10^{-11} cm^3 molecules^{-1} s^{-1}	Rate coefficient of HO_2 + OH[66]
$k_{HO2+HO2}$	1.7×10^{-15} cm^3 molecules^{-1} s^{-1}	Rate coefficient of $HO_2 + HO_2$[66]
$K_{hydration}$	Structure activity relationships	Equilibrium Constant for R=O $\leftrightarrow$ R(OH)$_2$[f]

846[a] Pseudo first order rate coefficient was computed using the Henry's Law constant[77] of 0.0138 and a rate
847coefficient[76] for $RO_2 + O_2$ of 2.5 x 10^{-12} cm^3 molec^{-1} s^{-1}

848[b] Computed via structure activity relationships described in Refs. [78-79] Values for all the other species in the
849reaction (Table S1 in the SI) are similarly calculated and fall in the range of $10^{-14} - 10^{-13}$ cm^3 molecules^{-1} s^{-1}
850.

851[c] The $RO_2 + HO_2$ rate coefficient in the aqueous phase is estimated using the 2-3 times difference in the
852rate coefficient[80] from $HO_2 + HO_2$ observed in the gas phase.[81-82] Peroxy-peroxy rate coefficients in
853solution can span a large range, and the values used here are at the lower end of the range. The sensitivity
854of the results to values set to the high end of the range is discussed in the SI (See section S6, Scenario 4).

855[d] Rate coefficient used is consistent with values (~ 10^{-12} cm^3 molec^{-1} s^{-1}) reported in Refs. [80, 83]

856[e] This rate coefficient is that for abstraction of H from the carboxylic acid group in oxalic acid.

857[f] The equilibrium constants for hydration reactions were calculated from the structure activity
858relationships and are listed in Table S1 in the SI. (see Ref. [60]) As described for acid-base chemistry, this
859equilibrium constant was folded into an effective rate constant.

860

862

863

864

865

Table 2: Model Scenarios

| Scenario	Free Radical	Acid-Base	Evaporation of C_2 Fragments
1	✔	✘	✘
2	✔	✔	✘
3	✔	✔	✔

Table 3: Decay Constant Comparison: Experimental and simulated reaction rate constant of CA. Coefficient of determination values (R^2) are calculated for the model scenarios to validate the exponential fit. Note that only scenario 3 has a reaction rate constant value within experimental error.

Model Scenario	$k_{obs} ¿ cm^3 s^{-1} molec^{-1}$	R^2
Experiment	$(5.27 \pm 0.28) \times 10^{-13}$	
1	4.68×10^{-13}	.99
2	6.08×10^{-13}	.99
3	5.38×10^{-13}	.99

874
875

876
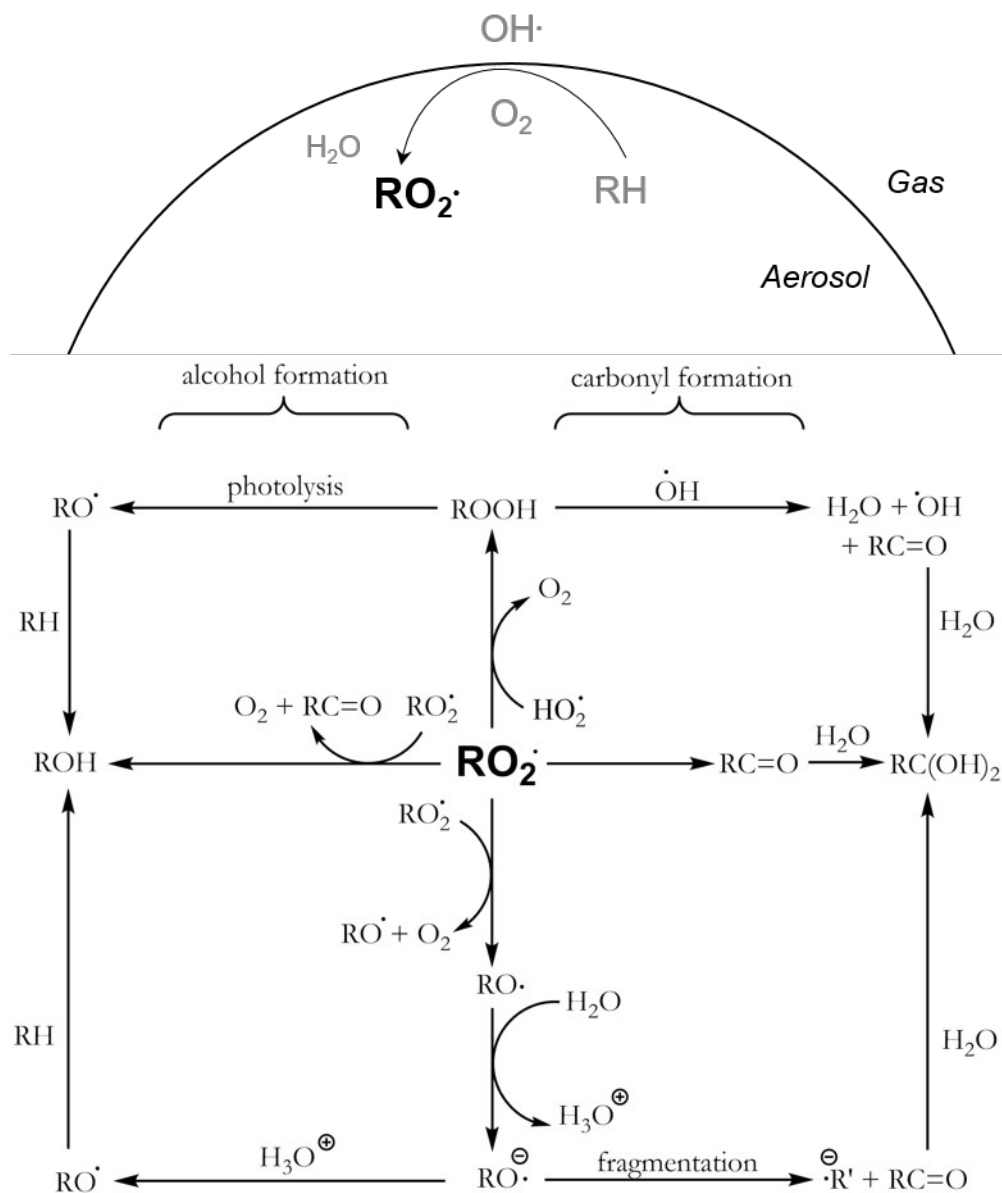
Figure 1: Reaction pathways of RO_2 to yield functionalized and/or fragmented products. A diagram of the free radical, pathways of RO_2 and subsequent acid-base and hydration reactions used to model the heterogeneous oxidation of aqueous citric acid aerosol by OH radicals. The left and right branches of the RO_2 reactions generate functionalized organic products. The top and bottom branches not only promote free radical cycling, but lead to bond cleaving reactions that produce lower weight, more functionalized reaction products. The RO fragmentation channel is significantly activated by an adjacent functional group and/or the deprotonation of a carboxyl group in the radical, as suggested by *ab initio* calculations (see text for details).

885

886

887

888

889

890

Scheme 1
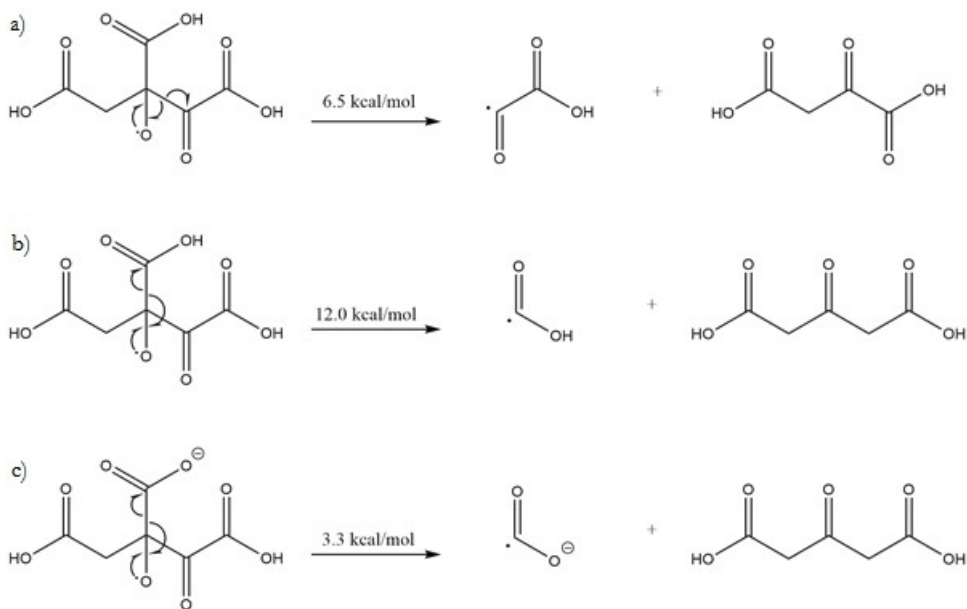
891

892

893

Scheme 2
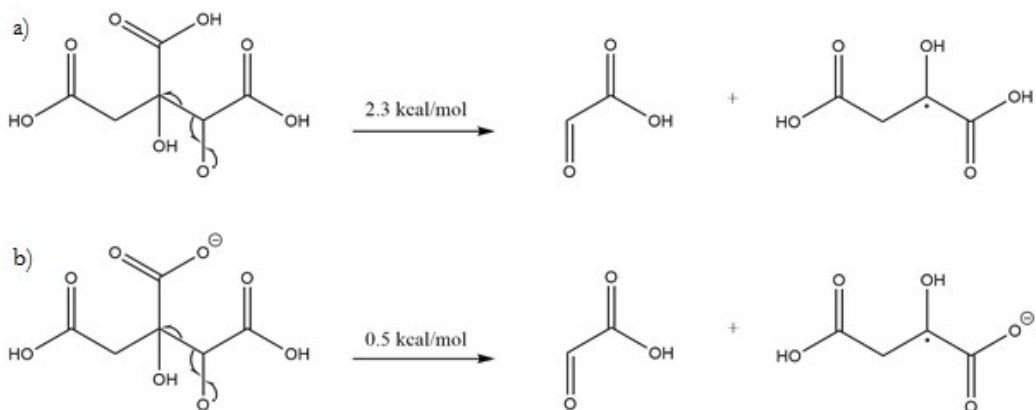
894

895

896

897

898

899

903
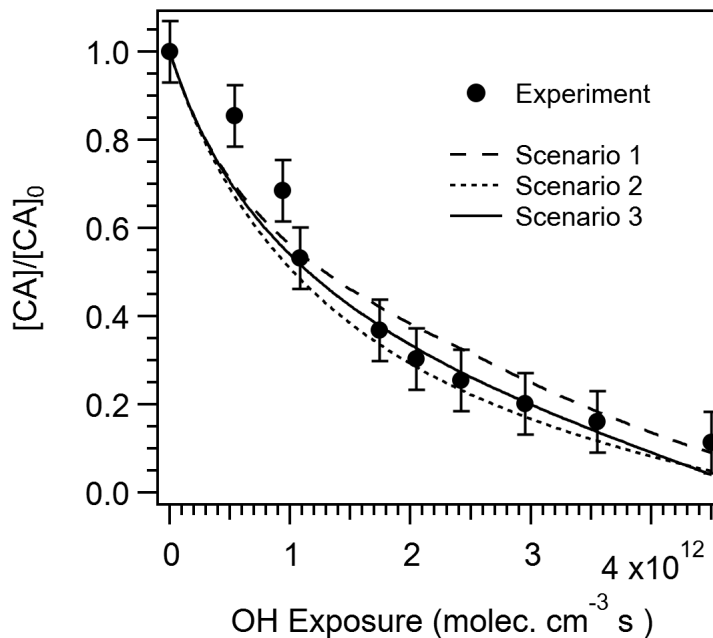
Figure 2. Experimental and simulated reactive decay of CA as a function of OH exposure. The experimental and simulation results were normalized to unreacted $[CA]_0$ prior to heterogeneous reaction. See Table 1 for simulations parameters and Table 2 for scenario descriptions.

907

908

909

910

911

912

913

914

915

916

917

918

920

921

922
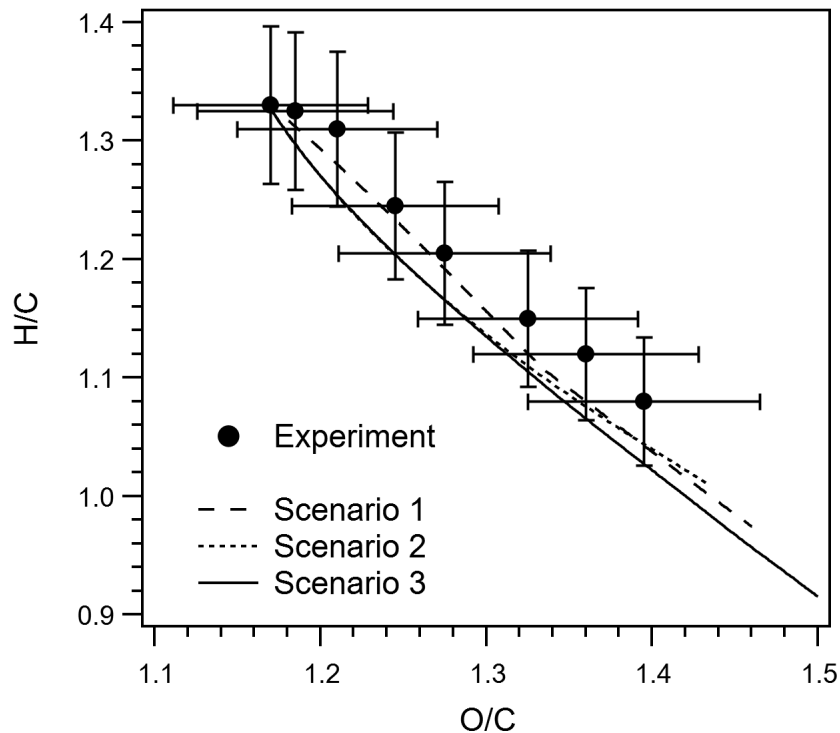
Figure 3. Experimental and simulated Van Krevelen plots (H/C vs. O/C) of average aerosol elemental composition. Simulation results fall within experimental error regardless of the model scenario. Note unreactive CA has H/C = 1.33 and O/C = 1.16. As the reaction progress the average H/C of the aerosol decreases and the O/C increases.

927

928

929

930

931

932

933

934
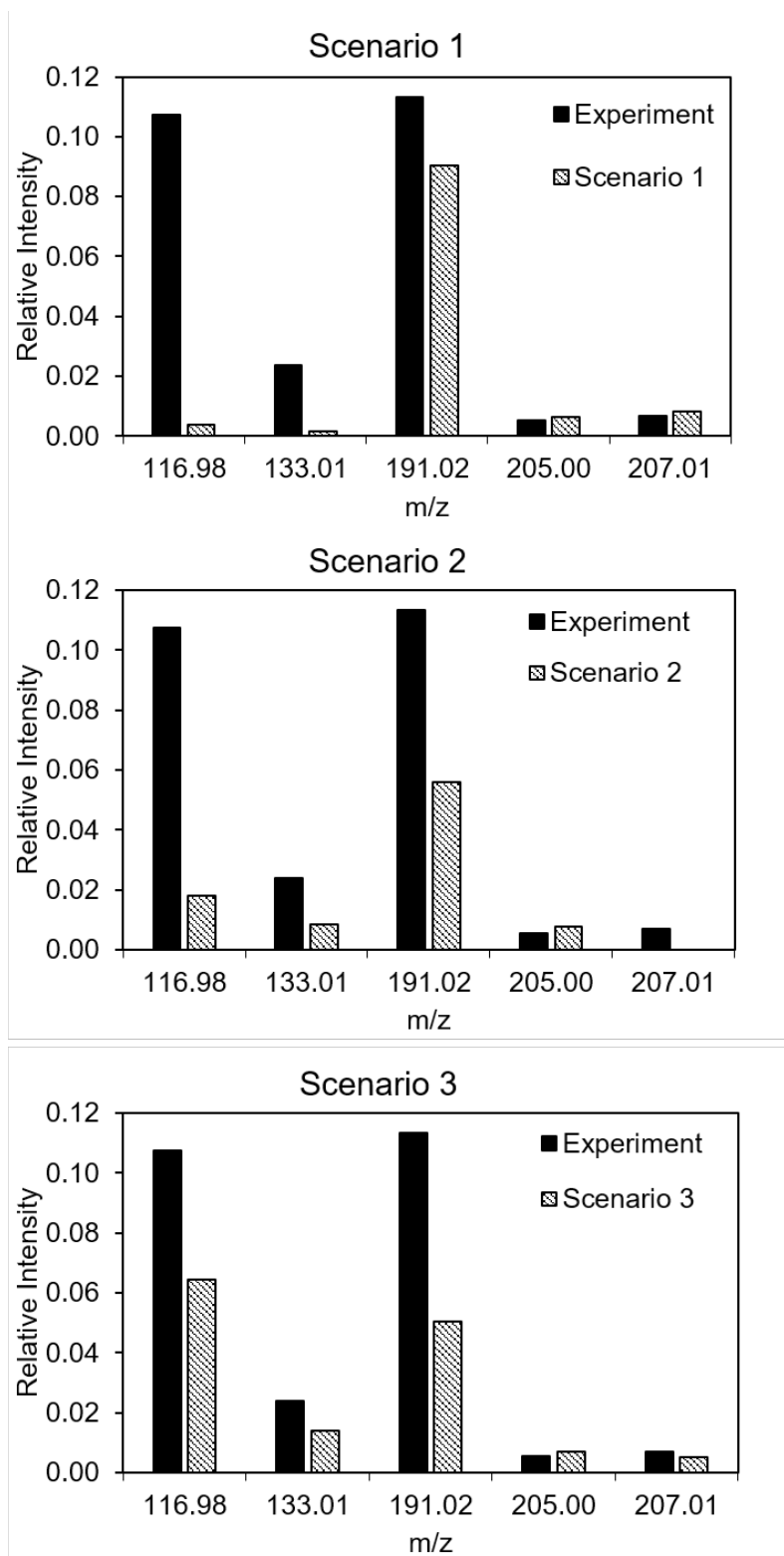
Figure 4. Experimental and simulated negative ion mass spectra of the major oxidation products of CA produced at an OH exposure of 4.4×10^{12} molecules s cm^{-3}. See Figure 5 for structures of these reaction products.

m/z	-ve ion	Structure	pKa	O/C	H/C
73.03	C_2HO_3		3.32	1.50	1.00
116.98	C_3HO_5	Mesoxalic acid	1.15	1.67	0.67
119.00	$C_3H_3O_5$		1.98	1.67	1.33
133.01	$C_4H_5O_5$	Malic Acid	3.40	1.25	1.50
191.02	$C_6H_7O_7$	Citric Acid	3.13	1.17	1.33
205.00	$C_6H_5O_8$		2.23	1.33	1.00
207.01	$C_6H_7O_8$		2.90	1.33	1.33

Figure 5: Molecular structures, negative ion m/z, H/C, O/C and pK_a of the major reaction products observed experimentally by Davies and Wilson.[37]
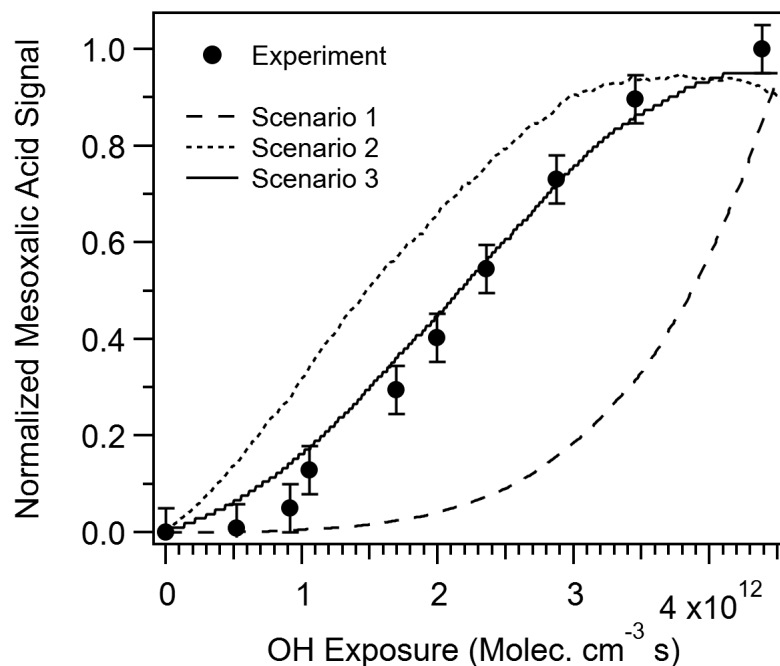
948**Figure 6:** Experimental and simulated concentration of mesoxalic acid (m/z = 116.98) as 949function of OH exposure. For comparison the experimental and simulated concentration was 950normalized to the maximum value. Scenario 3 predictions are within experimental error.

951

952

953

954

955

956

957

958

959

960

961
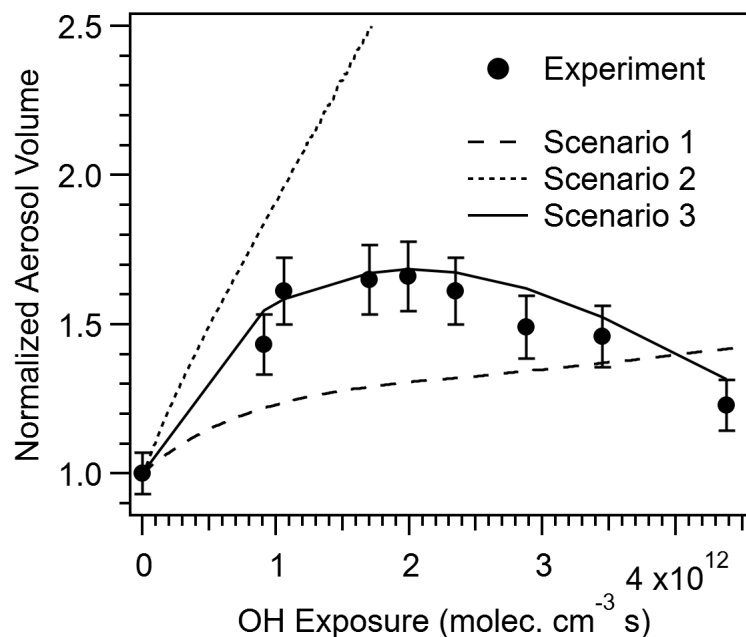
Figure 7: Experimental and simulated normalized aerosol volume as a function of OH exposure. The volume is normalized to the unreacted CA aerosol. The rapid growth observed in Scenario 2 is due to lack of evaporation in this scenario. Scenario 1 fails to capture the initial increase in volume and similar to scenario 1, does not predict the decrease in volume due to a lack of evaporation. Scenario 3 is the only model to predict within experimental error the complex growth and decay in aerosol volume observed over the course of the reaction.

972

973

974

975

976

977

978

979

980

981

982

983

984
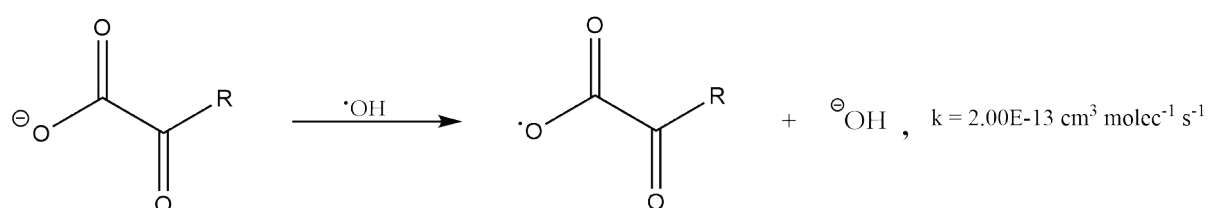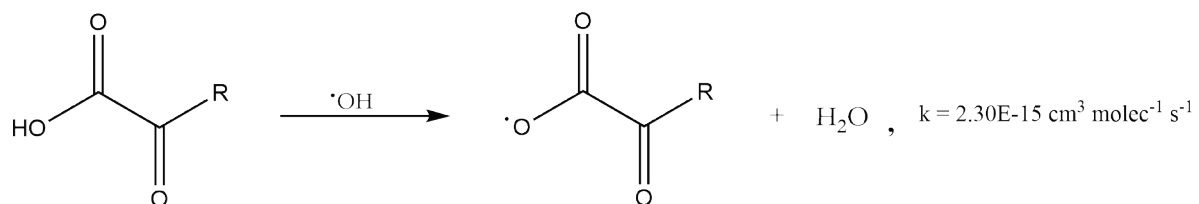
985

986**Figure 8:** A comparison in acyloxy radical formation rate between an α-keto acid and its 987conjugate base. The charge transfer reaction of the base (bottom) has a rate coefficient that is 988approximately 2 orders of magnitude larger than the hydrogen abstraction reaction on the acid 989(top). The inclusion of acid-base chemistry substantially increases acyloxy radical formation 990rates.
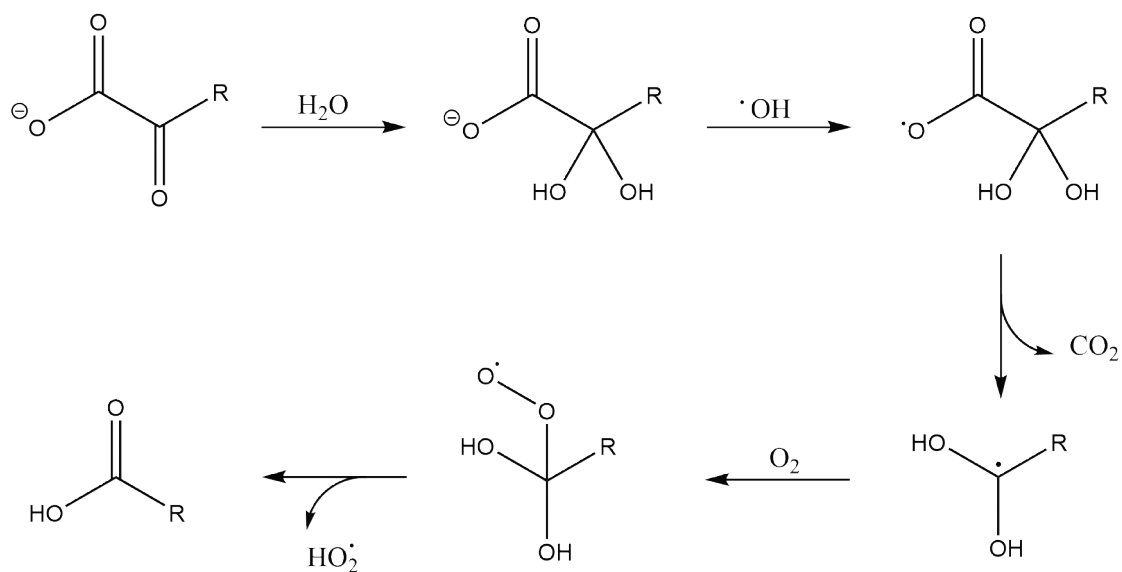
991

992

993

994

995

996

997

998

999

1000

1001

1002

1003

1004

1005

1006

1007

1008

1009

1010**Figure 9:** Carboxyl group formation accompanied by one-carbon loss via acyloxy radical 1011formation. After decarboxylation of the acyloxy radical, addition of oxygen to the resulting 1012alpha-di-hydroxyalkyl radical and subsequent decomposition yields an acid that differs only by 1 1013carbon atom from the original reactant. Hydration is an essential part of this pathway, making it 1014unique to the aqueous-phase.
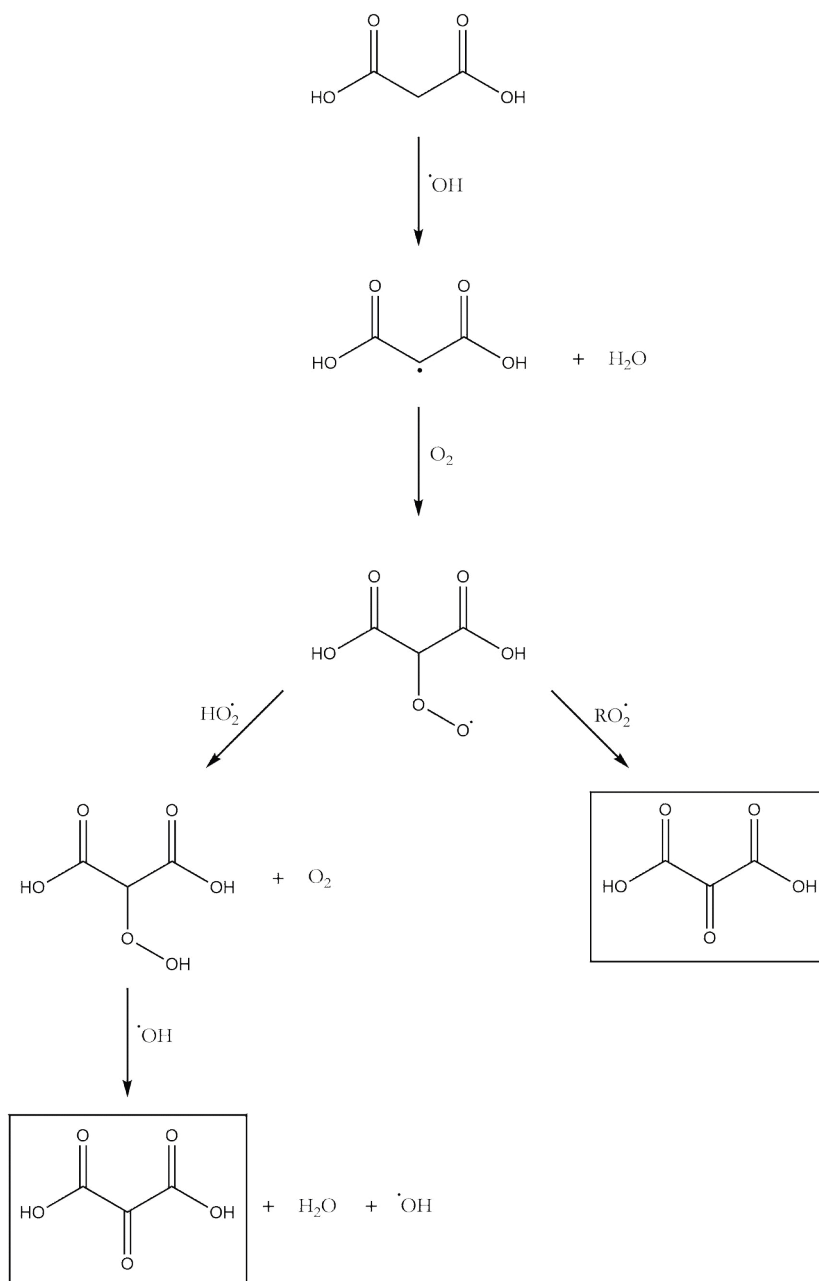
1015

1016

1017

1018

1019

1020

1021

1022

1023**Figure 10:** The two reaction pathways that produce mesoxalic acid (m/z = 116.98). In the right 1024branch, RO_2 may also react to yield 2-hydroxymalonic acid (i.e. $C_3H_4O_5$, tartronic acid). The 1025ROOH+OH reaction in the left branch regenerates OH further propagating the reaction.
1026
1027
1028
1029
1030
1031
1032
1033

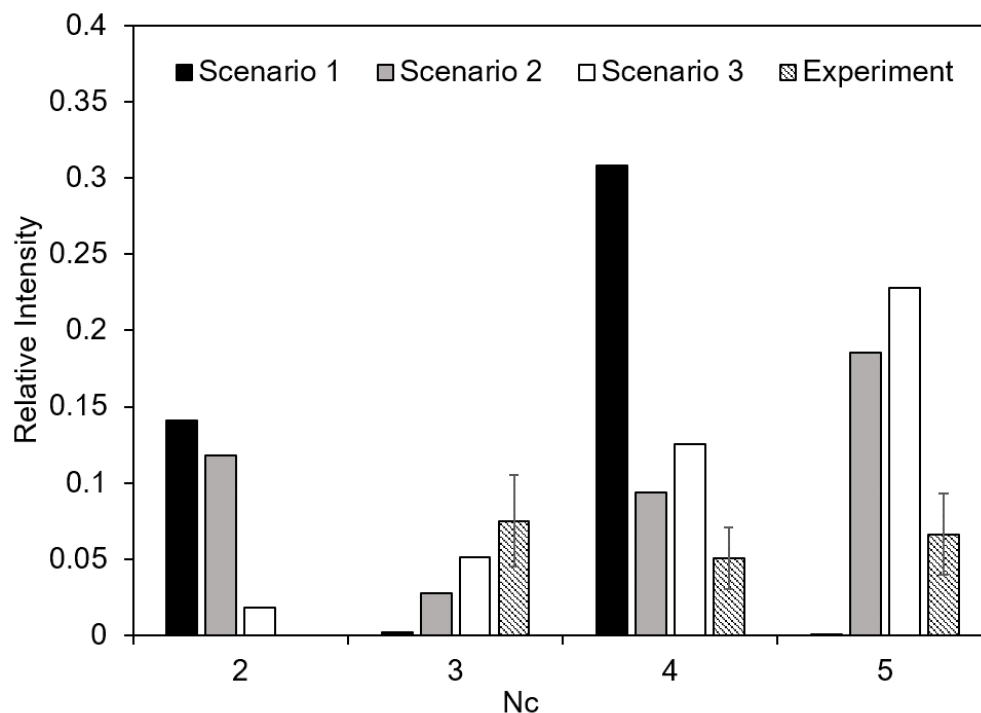1040**Figure 11:** Simulated product carbon number (N_c) distributions (at OH exposure = 2.2 x 10^{12} 1041molec. cm^{-3} s) for Scenarios 1, 2 and 3. The experimental data are also shown at OH exposure = 10422.1 x 10^{12} molec. cm^{-3} s, for qualitative comparison to the calculations. Each carbon number is 1043computed by dividing the sum of all species corresponding to a carbon number by the initial 1044concentration of CA. Scenario 1 lacks C_5 products, which are only produced when acid-base 1045chemistry is included in the reaction scheme (i.e. Scenario 2 and 3).
1046

1047
1048
1049
1050
1051
1052
1053
1054
1055
1056
1057
1058

95
96

1059
1060
1061
1062
1063
1064
1065
1066
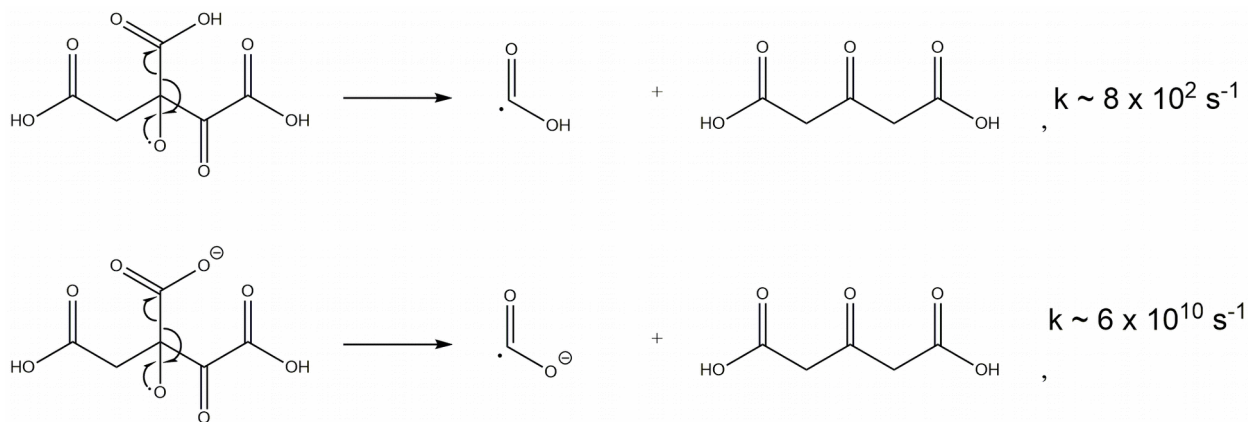
1067

1068**Figure 12:** Computed rate coefficients for the unimolecular decomposition of alkoxy radicals
1069(see text for details). Fragmentation of the radical anion (bottom) is many orders of magnitude
1070faster than the neutral case (top).
1071
1072
1073
1074
1075
1076
1077
1078
1079
1080
1081
1082
1083
1084
1085
1086
1087
1088
1089
1090
1091
1092
1093
1094
1095
1096
1097
1098

97   49
98

1099
1100
1101
1102
1103
1104
1105
1106
1107
1108
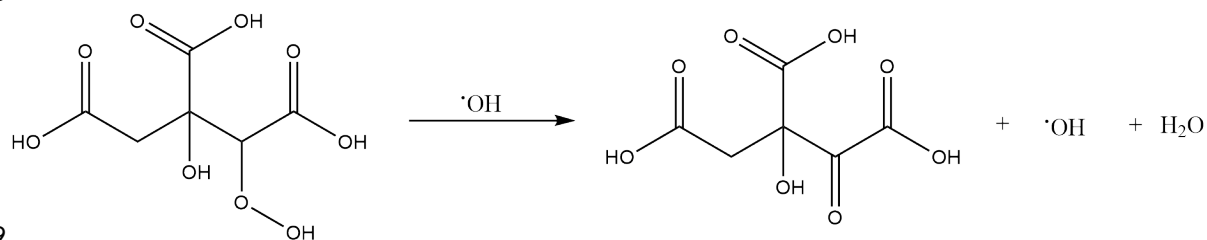
1109

1110**Figure 13:** A significant reaction pathway that converts a ROOH group into a carbonyl with H_2O
1111and OH as coproducts.
1112
1113

1114

1115

1116

1117

1118

1119

1120TOC Graphic

1121

1122

1123

1124

1125